Dynamic Modeling and Parameter Identification of a Plug-in Hybrid Electric Vehicle

by

Sindhura Buggaveeti

A thesis
presented to the University of Waterloo
in fulfillment of the
thesis requirement for the degree of
Master of Applied Science
in
Systems Design Engineering

Waterloo, Ontario, Canada, 2017

I hereby declare that I am the sole author of this thesis. This is a true copy of the thesis, including any required final revisions, as accepted by my examiners.

I understand that my thesis may be made electronically available to the public.

Abstract

In recent times, mechanical systems in an automobile are largely controlled by embedded systems, called micro-controllers. These automobiles, installed with micro-controllers, run complex embedded code to improve the efficiency and performance of the targeted mechanical systems. Developing and testing these control algorithms using the concept of model based design (MBD) is a cost-efficient and time-saving approach. MBD employs vehicle system models throughout the design process and offers superior understanding of the system behaviour than a traditional hardware prototype based testing. Consequently, accurate system identification constitutes an important aspect in MBD. The main focus of this thesis is to develop a validated vehicle dynamics model of a Toyota Prius Plug-in hybrid vehicle. This model plays a crucial role in achieving better fuel economy by assisting in the development process of various controller designs such as energy management system, co-operative adaptive cruise control system, and trip planning module.

In this work, initially a longitudinal vehicle dynamics model was developed in MapleSim that utilizes acausal modeling techniques and symbolic code generation to create models that are capable of real-time simulation. Here, the motion in longitudinal direction was given importance as it is the crucial degree of freedom (DOF) for determining the fuel consumption. Besides, the generic and full-fledged vehicle dynamics model in Simulink-based Automotive Simulation Models (ASM) software was also modified to create a validated model of the Prius. This software specifically facilitates the implementation of the model for virtual data collection using a driving simulator. Both vehicle models were verified by studying their simulation results at every stage of the development process.

Once the vehicle models were fully functional, the accurate and reliable parameters that control the vehicle motion were estimated. For this purpose, experimental data was acquired from the on-road and rolling dynamometer testing of the Prius. During these tests, the vehicle was instrumented with a vehicle measurement system (VMS), global-positioning system (GPS), and inertial measurement unit (IMU) to collect synchronized vehicle dynamics data. Parameters were identified by choosing a local optimization algorithm that minimizes the difference between simulated and experimental results. Homotopy, a global optimization technique was also investigated to check the influence of optimization algo-

rithms on the suspension parameters.

This method of parameter estimation from on-road data is highly flexible and economical. Comparison with the parameters obtained from 4-Post testing, a standardized test method, shows that the proposed methods can estimate parameters with an accuracy of 90%. Moreover, the longitudinal and lateral dynamics exhibited by the developed vehicle models are in accordance with the experimental data from on-road testing. The full vehicle simulations suggest that these validated models can be successfully used to evaluate the performance of controllers in real time.

Acknowledgements

Firstly, I would like to thank my supervisors Prof. John McPhee and Prof. Nasser Lashgarian Azad for their tremendous support, guidance and motivation provided throughout my master's degree. In addition, I wish to thank Prof. Krzysztof Czarnecki and Prof. Eihab Abdel-Rahman for their insightful feedback on improvement of this thesis.

I would like to thank Toyota and Automotive Partnerships Canada as sponsors of this research. I would also like to acknowledge the assistance of Toyota Motor Manufacturing Canada (TMMC) engineers, Rich Young, and Adam Howard, during track testing.

My special thanks to Matthew Van Gennip, Chris Shum, and Stefanie Bruinsma for the vehicle instrumentation support and continuous collaboration without which experimental data collection would have been impossible.

I am very grateful to all my colleagues in Motion Research Group and SHEVS lab for creating a healthy atmosphere for research. I would like to extend my appreciation to Mohit Batra and Amer Keblawi for helping me understand and quickly resolve various problems encountered during various phases of this research. Mahyar Vajedi and Bijan Sakhdari are acknowledged for the support provided during data collection, and Sadegh Tajeddin for setting up the driving simulator.

Lastly, my heartfelt thanks go to my parents and friends for their unconditional support throughout all these years.

Dedication

This is dedicated to my parents.

Table of Contents

List of Tables

List of Figures

Chapter 1

Introduction

1.1 Motivation

Air pollution is caused by the release of noxious gases such as carbon monoxide, sulphur dioxide, nitrous oxide, and chemical vapours. Besides giant factories, the greatest contributor to pollution is automobile emissions, produced mainly from cars. According to the U.S. Department of Transportation, from 1970 to 2010 these emissions have been exacerbated with the tripling of vehicle miles traveled. Such sharp increase in the traffic volume spurred questions over the impact of the automotive industry on the environment and the ozone layer. This led many governments to strengthen their fuel efficiency regulations several times in recent years, in an effort to reduce the environmental and economic costs associated with burning gasoline.

To address this growing concern over environmental pollution and gasoline prices, over the past few years the automotive industry has undergone a major shift from conventional vehicles (CVs) to plug-in hybrid electric vehicles (PHEVs) and battery electric vehicles (BEVs). Although battery electric vehicles have higher efficiency over PHEVs, limited driving range, availability of public charging stations, and higher upfront costs made PHEVs a viable option over BEVs for the short term.

Unlike conventional vehicles that are solely powered by an internal combustion engine,

PHEVs have an internal combustion engine and an electric motor/generator. The vehicle can be powered partially or wholly by either of them. These other sources of energy in PHEV powertrains allow the engines to be smaller and more efficient, which translates into lower emissions. Since PHEVs come with batteries that can be recharged by plugging them into an external power source, the vehicle can travel further in pure electric mode making it achieve better fuel economy over hybrid electric vehicles (HEVs). Regenerative braking is another fuel-saving feature associated with PHEVs that allows some of the vehicle's kinetic energy during braking to be captured, turned into electricity, and stored in the batteries. Ultimately, the actual fuel economy for PHEVs depend on their powertrain operating mode, which is governed by the energy management system (EMS). The EMS acts as the heart of the PHEV by playing an important role in determining the amount of power delivered by each energy source. Hence, it is essential to have an efficient energy management control strategy to achieve the best fuel economy.

1.1.1 Model based control design

Smart vehicle systems run a million lines of embedded code to implement control strategies for advanced propulsion, navigation and safety features [1]. As these vehicles grow with functionality, the software embedded in them grows significantly. But, developing such complex control code and testing it directly on a vehicle prototype is not a cost-efficient approach. There is a high risk that the physical prototype could be damaged if the software running on electronic control unit (ECU) encounters a bug and behaves abnormally. Such damage causes further delays in testing, and requires huge effort to fix the prototype. In response to these concerns, the automotive industry began researching solutions that can lower the development cost of these smart vehicles.

Model based control design has been found to be a cost-efficient and time saving approach that can resolve the key issues associated with testing of controllers. In this, errors are detected in the early stages of controller design, thereby minimizing the cost associated with faulty ECUs. The process of testing starts by converting the designed control algorithm model to C code through code generation, which eliminates hand coding errors and enables the code to be quickly deployed on the hardware processor. Similar code genera-

tion is done for the high-fidelity model of the vehicle to accelerate simulation by running it on a real time computer. Consequently, error detection is done by continuously evaluating and validating controller design on real time vehicle simulation model through hardware in loop (HIL) setup as shown in Fig. 1.1 [2]. HIL simulation ensures that the controller is real time implementable by responding to the fast dynamics of the vehicle simulation model. In this manner, issues related to the developed control algorithm can be resolved in the initial stages of design. Subsequently, the optimized and validated controller that has undergone continuous HIL testing during the development process can be confidently deployed on a prototype vehicle's hardware platform.

From the above mentioned process, it is understood that developing a validated full vehicle simulation model to implement and test the controller is as important as designing a controller strategy. Also, it must be accurate enough to reproduce the behaviour of the vehicle on which the controller is going to be implemented. Modeling a vehicle is especially complicated when it has multiple components such as engine, motor, generator, batteries, inverter, and vehicle dynamics. Hence, the full vehicle model has to be developed by various specialists who use simulation to design and add details to these subsystem models. All these detailed models will then be integrated back into system level realization and verified through simulation.

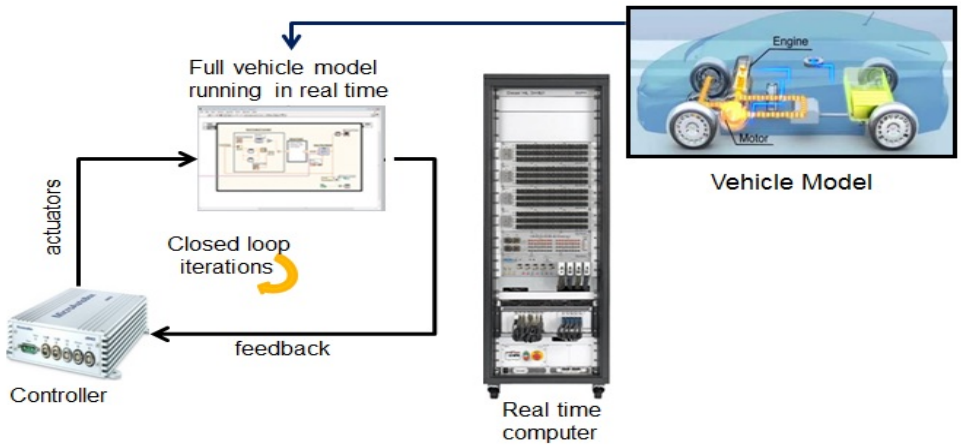

Figure 1.1: Hardware-in-loop setup

This research forms a part of model-based design of a real-time energy-optimal con-

troller for a Toyota Prius PHEV 2015. This controller consists of trip planning module, route based energy management system and eco-cruise controller that coordinate to minimize total energy cost, including both fuel and electrical energy taken from the grid [3]. To evaluate and validate the actions of various predictive strategies associated with these controllers, it is necessary to have a validated high-fidelity simulation model of the Prius PHEV 2015 with complete powertrain and vehicle dynamics.

1.1.2 Driving simulator

Driving simulators have also become an important development tool in automotive research. They are not just limited to research purposes, but are also used in the development process of a vehicle by either the car manufacturers or their suppliers. Driving simulators are mainly used to study how a vehicle responds in an accident, their reliability and their energy efficiency while considering all possible influences on the vehicle. These simulators took testing new control software to the next level by allowing the researchers to visualize behavior of virtual cars for different maneuvers, drivers, road conditions and traffic situations. This resulted in a safe, convenient and quick testing in comparison to prototype cars.

The driving simulators come with a vehicle dynamics simulation package that provides realistic vehicle behavior simulation in real time. This research also deals with the validation of vehicle dynamics model in the driving simulator to facilitate its usage for the purpose of data collection from multiple virtual sensors in a traffic simulation. The data collected from virtual vehicle simulation in rare driving scenarios can be used in the robustness analyses of various controller designs.

1.2 Objectives

The main focus of this research is to develop a validated longitudinal vehicle dynamics model of Prius PHEV 2015, which forms the most important degree of freedom for controllers that aim at minimizing fuel consumption. The other goal is to modify and tune

the generic vehicle dynamics model in Automotive Simulation Models (ASM) software for the driving simulator, so that it replicates the behavior of the Prius in longitudinal and lateral maneuvers. Parameters necessary for validation of both models will be identified by processing the data obtained from the Prius equipped with multiple sensors in real road driving maneuvers.

1.3 Thesis organization

This thesis is organized into 7 chapters. The first describes the motivation behind this research and main goals of this work. Chapter 2 presents the literature review to achieve the goals laid out in Chapter 1. Chapter 3 discus the development of a high fidelity vehicle dynamics model in MapleSim using multibody dynamics and also modifications done to the ASM generic vehicle dynamics simulation model in driving simulator to match the vehicle dynamics characteristics of Toyota Prius. Chapter 4 presents the test vehicle, experimental setup, maneuvers performed, and test facilities used during vehicle testing for collecting experimental data. Chapter 5 presents different methods used in this research to extract the vehicle parameters from the experimental data of the vehicle testing described in the previous chapter. In Chapter 6, the parameters estimated in the previous chapters are supplied to the vehicle dynamics models in MapleSim and ASM simulation package. The accuracy of models is examined by further comparing the simulation results of these models against experimental data. The thesis concludes with Chapter 7, which presents the summary of research performed and identifies potential areas for future research.

Chapter 2

Literature review

Vehicle dynamics is a part of engineering that deals with the motion of a vehicle and the forces affecting this motion. Modeling of four wheeled vehicles has been studied extensively for the last 50 years. Analytical approach for understanding and modeling vehicle dynamics is preferred by many engineers as it describes the mechanics of interest based on the known laws of physics. However, before the computers were invented, analytical methods for solving problems with large number of subsystems and non-linearities in a vehicle were limited by the mathematical complexity.

Today, availability of computers with huge computational power and most of the problems associated with analytical approaches have been resolved. Computer simulation has significantly reduced the time and cost of designing and testing dynamic models of vehicle systems, thereby becoming a preferred tool over real world testing. Dynamic characteristics of vehicles are well understood and validated models have been developed through simulation for many applications. Standard terminology and coordinate systems have been laid to maintain consistency. Major types of computer-based tools for vehicle dynamics simulation are identified [4] and categorized as follows: purpose designed simulation codes, multibody simulation packages that are numerical, multibody simulation packages that are symbolic and toolkits such as MATLAB.

First half of this chapter reviews different software available for vehicle dynamics modeling for implementation in real time. Second half in this chapter introduces parameter

identification in dynamic systems, different optimization methods and presents standard methods used to identify vehicle dynamics parameters.

2.1 Multi-body vehicle dynamics modeling

Multibody dynamics has been used widely for the simulation and dynamic analysis of all kinds of vehicle systems. It involves modeling and studying the dynamic behaviour of a vehicle system in the form of links/rigid bodies connected together by joints. There are multiple computer-based tools for performing multibody dynamics analysis of which the most popular ones are Adams, CarSim, SimPack and MapleSim. Although there are several other techniques to model the dynamics of vehicles that can be found in the literature, they haven't achieved widespread usage commercially.

ADAMS: ADAMS is the most popular multibody simulation package to model, simulate and analyze complex dynamic systems. Its add-on package ADAMS/Car is especially geared towards vehicle dynamics simulation. It made vehicle modeling simpler by offering predefined templates for different vehicle components, suspension and steering configurations. However, addition of multi-domain subsystems (for example, a hybrid electric car requires modeling of both electric and mechanical subsystems/components) to ADAMS/Car is quite cumbersome and expensive. Also, validating the detailed vehicle dynamics model in ADAMS/Car is difficult as it requires information about several hard points, a parameter set that contains physical measures of geometry and joint locations. A few authors [5, 6] suggested that correlating experimental data with the ADAMS/Car model was a time consuming process. Besides this, these models solve large number of differential-algebraic equations numerically and are not suited for real-time applications due to their computational inefficiency.

CarSim: CarSim is a commercially available vehicle simulation package that provides accurate and computationally efficient methods for simulating the dynamic behavior of passenger cars, race cars and light-duty trucks [7]. It is based on AUTOSIM, which was developed with the goal of generating real-time simulation code from symbolic computation of multibody vehicle models. CarSim consists of a large library of detailed and validated

math models for all vehicle combinations that are capable of running faster than real-time. In CarSim, automobile subsystems are not modelled using geometric links. Instead, it uses look-up tables and parameters obtained from published-data, engineering tools and test rigs. For example, it does not consist of a multi-parameter tire model to simulate the dynamic behavior of tire for various slip-angles and loading conditions; instead it has a look-up table to simulate this non-linear behaviour of tire. Similarly, a suspension model can be fully defined using the data from a Kinematics and Compliance (K&C) test rig, or from virtual K&C testing of a high-fidelity simulation model developed in ADAMS/Car. This made modelling in CarSim simpler and resulted in faster simulation times. However, it has several disadvantages that limited its usage in research. This software is not capable for research dedicated towards specific subsystems in vehicle as it accepts only pre-defined list of input and output variables and manipulating equations is limited. Similar to ADAMS/Car, it doesn't facilitate multi-domain modeling. Also, obtaining data for look-up tables that are necessary for vehicle simulation requires testing of the vehicle at standardized test rigs, that might be either inaccessible or expensive.

MapleSim: MapleSim is a multi-domain, system level modeling and simulation tool based on graph theoretic methods. Graph theory was at first introduced by Leonard Euler [8] in 1736 and has been used since then by many researchers and engineers [9, 10] for modelling physical systems. MapleSim automatically generates governing equations of motion from system description in a systematic way based on vector-network method [11], which is a combination of vector dynamics and graph theory concepts. This method starts by examining how different bodies are connected in a multi-body system, generation of cut-set and circuit equations and substituting these constitutive equations into fundamental equation set. Shi and McPhee [12] described the application of this graph theoretic method to flexible multi-body and mechatronic systems. Schmitke et al.[13] used graph theory and symbolic computing to create efficient models specifically for multi-body vehicle dynamics.

MapleSim uses extensive math solvers and simplification technologies to reduce development time, and produce fast and high fidelity simulations. Unlike other physical modeling and signal flow modeling tools that are based on numeric formulation of the model, MapleSim is built on Maple, which enables us to perform symbolic computation and gives deeper insight into the system behavior, compared to tools like CarSim, by providing ac-

cess to model equations. It supports assessing the correctness of the model by allowing us to visualize the model equations in the form of differential equations, transfer functions or matrices in Maple. The equations with design parameters can be manipulated and post-processed to perform frequency analysis, sensitivity analysis and linearization. Banerjee et al.[14] has performed sensitivity analysis using graph-theoretic approach in MapleSim for multi-domain systems such as hydrodynamic torque converter, NiMH battery and a double wish-bone suspension.

Most software achieve real-time simulation by trading off model fidelity for model speed, whereas MapleSim generates simpler set of equations by performing algebraic manipulations and index reduction. Code generation tools that extract common sub-expressions are employed to further optimize these simplified equations for real-time implementation. Although CarSim does symbolic code generation, it is incapable of doing it for multi-domain models, and is not as flexible as MapleSim [13].

Customized vehicle dynamics models can be built easily from scratch utilizing Multibody component library in MapleSim. Previously, Hall et al.[15] developed a reduced 10 DOF full vehicle model in MapleSim and compared its dynamic response against the high-fidelity model of a sports utility vehicle in ADAMS/CAR. They showed that the reduced model's response matches that of the multi-link in ADAMS/Car when it was tuned with parameters obtained from homotopy optimization. Thagavipour et al.[16] developed a high-fidelity power train model of a Toyota Prius 2015 in MapleSim, but much focus was not given to the layout and validation of its vehicle dynamics model.

2.2 Driving simulators in vehicle research

The thought of reducing the operational cost over the use of actual equipment led to the development of simulators for flight simulation and training purposes before the Second World War. These simulators were adopted and operated for highway driving research in 1960s [17] with the advent of visual displays and powerful computational technology. Since then, driving simulators have undergone major changes and currently evolved into systems that provide real time simulation with advanced visual, motion and sound systems to give

real road driving feel. Blana [18] conducted a survey on driving research simulators around the world and classified them into three categories according to their cost, which include:

Low-cost driving simulators: Growth in the PC technology made these simulators a reality. These driving simulators are low cost due to limited view, simple graphic displays or fixed-base. They offer sufficient fidelity in the visual and auditory cueing and are particularly cost effective for student researchers in university, manufacturers, and suppliers with limited budget and driver training.

Medium-cost driving simulators: These simulators can perform real-time simulation, have larger screens and full sized vehicle with controls. They have either a fixed-base (no feedback) or a simple moving-base system that can generate vibrations or pitching motions while driving.

High-cost driving simulators: These simulators are more advanced with high performance and data storage, 360° view from multiple synchronized PCs, sensors for feedback to driver, driver eye tracking technology, high fidelity motion platform with all six or more degrees of freedom. These are most common in the research and development facilities of large manufacturers like Daimler-Benz, Ford, Toyota, GM, Mazda etc.

There have been many attempts by researchers in constructing simulators with capabilities similar to that of mid-level research simulators at a lower cost [19, 20, 21]. However, they are mostly designed towards performing specific type of research and have some limitations. Depending on their capability, driving simulators are used for wide range of applications that range from designing vehicles by assessing driver's perception, research on emergency maneuvers, driving on different road surfaces, developing intelligent vehicle technologies to driver training, road ergonomics, and driving aids.

The major component of a driving simulator, irrespective of the application it is being used for, is its vehicle dynamics model. This model describes the vehicle motion based on the inputs from driver and environment using laws of physics. This vehicle motion can be felt by drivers through feedback from steering wheel torque and movement of motion platform in high cost driving simulators, whereas vehicle motion can only be visualized through the movement of a virtual vehicle model on graphical interface in low cost simulators. Most driving simulators use multibody vehicle dynamics models. Shiiba et al.[22]

discussed the advantages of using a multibody vehicle model in driving simulators by comparing the error generated in wheel alignment with a simple 5DOF mathematical vehicle model. Andreasson et al.[23] developed a high fidelity vehicle dynamics model for driving simulator utilizing the free Modelica standard library components and validated the real-time model against offline tool with respect to precision and accuracy. Dempsey et al.[24] also proposed a more complex Modelica based multi-body model for real-time simulation by considering the non-linearities in suspension models with bushings and volumetric tire contact model. However, these models for driving simulator are not physically validated against experimental data. Fernandez et al.[25] and Obialero et al.[26] developed vehicle dynamics models from scratch by formulating equations for each sub component using Dymola, a Modelica based software. The model parameters were tuned by comparing simulation results with experimental data of a Saab 93, until it performs like a real car. This kind of tuning without proper base/strategy is tedious especially when there are 75 parameters[26] and there is a chance that the tuned parameters might not be physically reasonable or might work for only specific data sets. Salaani et al.[27, 28, 29] performed extensive research on modeling and validation of vehicle dynamics models of 1994 Ford Tarus and 1997 Jeep Cherokee for driving simulators using real time recursive dynamics (RTRD). Besides these, there are some notable software packages that provide Simulink based vehicle models along with scenario and animation generation for driving simulators such as CarSim, ASM, and Dyna4. These software packages execute on real-time platforms such as dSPACE, Opal-RT, and National Instruments.

2.3 Parameter identification

In the context of engineering, a parameter is defined as a combination of physical properties that can help in determining or classifying the response of a system. Not all parameters of a system are constant and depend on the environment with which the system is interacting. A mathematical model with parameters that are specific to the system is often used to study and analyze the behavior of that system. However, most of the times, parameters are unknown and we only have the measured information about inputs and outputs of a system. Hand tuning the parameters of the system model to match output experimental data

requires no computational effort, but has many significant disadvantages [30] associated with it. It is extremely time consuming when multiple parameters have to be hand tuned to match multiple sets of measured data.

The methodology of building a mathematical system model from its input and output measurements is known as system identification. Major part of this process involves estimating the physically immeasurable system parameters, which is termed as parameter identification or parameter estimation. The problem of parameter identification can be posed an optimization problem, where the arguments of the global minimum of an objective function are the best parameter values that can be obtained. Parameter identification is a very common and well-researched topic that is encountered in many fields, including mechanical and mechatronic engineering, civil engineering, chemical engineering, aerospace, and material science.

Depending on the complexity of the vehicle model used, number of parameters that characterize its response can vary from 10 to as high as 100. The vehicle parameters that are constant, i.e., do not vary with time are generally estimated through offline estimation techniques by fitting the model output (simulated data) with experimental data. When the error between simulated and experimental data is linear in parameters, a closed form solution can be obtained and solved easily. However, when the error is non-linear in parameters, offline estimation algorithms are used which include Newton-Raphson, Gauss-Newton, Lavenberg-Marqdt, and genetic algorithm. As this is done offline, computational effort isn't a major issue. The parameters that change during model operation or time varying parameters are estimated using online estimation algorithms when the new data from the model is available [31]. This follows a Bayesian approach that uses probability to quantify the variation or uncertainty and unknown parameters are considered as random variables. As the parameters are estimated and updated during the model operation, estimation algorithm must be fast enough for real-time implementation. Extended Kalman filter, unscented Kalman filter and recursive non-linear least squares are some commonly used methods for on-line parameter identification. This estimation is used to achieve robustness with respect to disturbances such as measurement noises and modeling errors. Online parameter identification has become an integral part in the development of adaptive and robust controllers for obtaining good plant model and has found many applications.

In automotive field, this technique is often used while developing controllers for battery systems [32], tire-road friction [33], vehicle inertia [34], vehicle mass [35], and road grade angle [35] depending on the application for which controller is intended. However, this research only deals with off-line parameter identification using experimental data.

2.3.1 Off-line parameter identification

Off-line identification is used for model development and model validation during the initial phases of controller development and implementation. The model validated through off-line identification serves as a basis to obtain model which is appropriate for on-line use [31]. This research involves developing validated vehicle simulation model, which brings in the need for estimating its parameters.

All parameters are necessary for the multibody vehicle model to function. But when the model is complex, which is in this case, estimating all the parameters at once is not a good approach and leads to invalid or noisy or biased parameter values [36]. In this case, a modular approach is often followed, where specific parameters are found through various identification techniques by choosing the data sets that excite these values. There are many advanced test facilities that are designated to excite the vehicle and identify parameters such as location of center of gravity, inertia, suspension parameters, road load parameters and tire parameters.

Center of gravity (CG): Longitudinal and lateral location of center of gravity of a vehicle can be found easily by measuring loads on all tires through load scales. But, finding the height of center of gravity is not so straight forward. One of the oldest and most popular method is to lift the front or rear tires to a certain height which causes shift in the CG location. This is known as modified reaction method. Height of center of gravity is obtained by taking moments about the tire contact point on the ground [37]. This method doesn't require any special equipment other than load scales. However, it is prone to inaccuracies from motion of fuel and lubricants, longitudinal force in the tire contact patch and others. In 1991, University of Michigan Transportation Research Institute (UTMRI) conducted a study [38] to assess different methods used by test facilities of General Motors, Ford, Chrysler and National Highway Traffic Safety Association (NHTSA) to determine CG

height. These facilities use more difficult test methods such as weight balance, null-point and pendulum methods, which also involve tilting the vehicle. All these methods provide more accurate estimate over modified reaction method, but require specialized equipment for testing. As an improvement over modified reaction method, Mango [39] proposed a more accurate method to estimate CG height by accounting for the effect of different loaded tire radii.

Vehicle inertia: Measurement of inertia isn't straight forward unless the body has uniform mass distribution and symmetricity around an axis. Most of the test facilities that can determine vehicle inertia [40, 41, 42] were initially designed to measure the location of center of gravity. Although these facilities differ in the special hardware used and methods of mounting, they are based on the same concept of rotating the vehicle about an axis and measuring the time period of oscillation to calculate inertia tensor. Rozyn et al.[34] used modal analysis for determining moment of inertia. Doniselli et al.[43] proposed a simpler arrangement by hanging the vehicle to a ceiling through four springs and allowing it to oscillate around an axis whose attitude changes continuously. However, this method requires additional post-processing to determine inertia tensor. Currently, vehicle inertia measurement machine (VIMM) and vehicle inertia parameter evaluation rig (VIPER) are the two advanced test rigs developed after many revisions [44, 45, 46] that can measure center of gravity location and inertia with high accuracy for light and heavy vehicles respectively.

Suspension characteristics: Component level testing through a damper test rig gives force velocity curve of damper by oscillating the damper according to predefined input signals. However, this kind of testing requires removal of damper from the vehicle and is more suitable in the initial stages of vehicle development. A 4-post test rig provides vehicle level testing, where the wheels are excited by random input signals or real road data. Accelerometers can be placed on the rims and body to relate and study how road inputs affect the sprung mass and unsprung mass of the vehicle [47, 48]. Another approach is kinematic and compliance testing shown in Fig. 2.1c [49], where the test data generated is used to obtain an accurate multibody model of suspension by adjusting the hard point locations and bushing stiffnesses [5, 6]. In this test, vehicle is bolted to a large table and forces are applied to tire contact patch along the axes that constrain and allow movement, from which kinematics and compliance properties are obtained. Although this test provides

results with high accuracy, it is more expensive than 4-post testing.

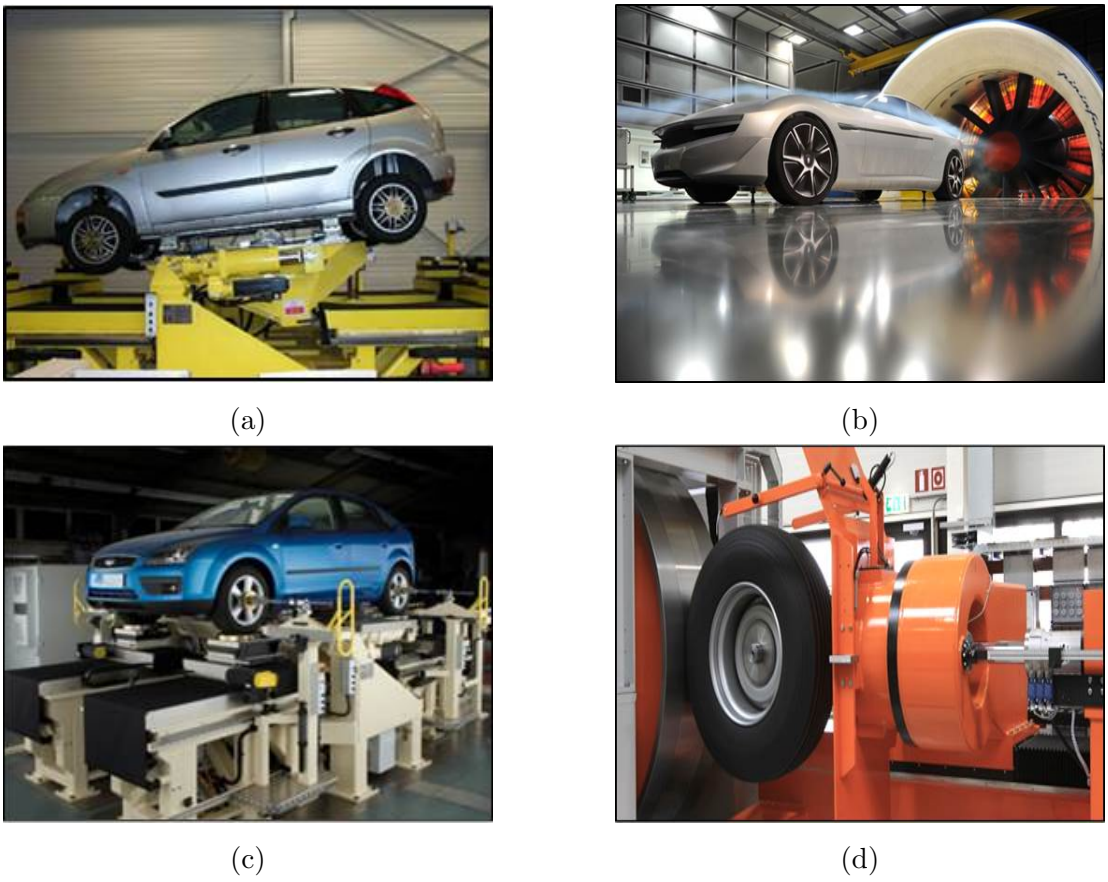

(a) (b)

(c) (d)

Figure 2.1: Advanced vehicle testing facilities: (a) Vehicle inertia and CG testing, (b) Wind tunnel testing, (C) Kinematics and compliance testing, and (d) Drum Tire testing

Tire testing: Initially, tire was considered as a suspension component and only vertical response was studied. Gradual growth in the importance of force and moment characteristics of tire led to the development of different tire testing methods. A drum testing machine shown in Fig. 2.1d [50], where tire rolls on a drum, is the oldest and commonly used rig to measure the tire characteristics. The major disadvantage of this method is that tires contact patch is curved according to the drum shape and is not an ideal way to test. To address this, a flat belt test machine was developed to measure force, moment, slip ratio,

slip angle, and rotational speed. But, this method failed to obtain the characteristics of tires while including the characteristics of suspension and steering. Over the past 15 years, on-road tire testing methods have become popular that use portable load sensors [51] to measure tire force and moment. This method can provide accurate information on how each tire behaves during acceleration, braking and steering while including the effects of suspension. However, flat belt testing is still used especially to study the combined slip characteristics of tires [52, 53].

Tire inertia is another important parameter due to its direct effect on wheel rotational speed. Most of the times it is obtained by considering tire as a solid cylinder with uniform mass distribution. But in reality most of the tire mass is concentrated near the edge. Unlike vehicle inertia which requires huge test setup due to heavy weight, tire inertia can be obtained easily by performing a pendulum test. Another approach is to roll the wheel over a ramp and record the time it takes to reach the bottom of ramp [54].

Drag coefficient: Traditionally, wind tunnel tests shown in Fig. 2.1b [55] are done in a controlled environment to measure aerodynamic-related characteristics of a vehicle. In this, air from a huge fan is allowed to move past a vehicle with a very high speed from different incident angles. This has become the standard test used by manufacturers to determine aerodynamics drag and lift coefficients from aerodynamic forces and pressure distribution on the vehicle. For smaller wind tunnel facilities, scaled models of vehicle can be used to measure the drag force [56]. Few authors performed computational fluid dynamics analysis (CFD) on scaled CAD models of the vehicle. However, accuracy of this method is highly dependent on how closely CAD model matches the real vehicle design. To understand the on-road aerodynamic performance of a vehicle, s are performed. With minimal instrumentation, drag coefficients can be obtained and these tests have shown good correlation with the data obtained from wind tunnel tests [57].

2.3.2 Optimization methods

The basic idea behind every parameter identification problem is nothing but solving an optimization problem, where the objective function is to minimize the difference between simulated and experimental values of a system. The arguments of this objective function

represent the parameters of the system. Depending on the algorithm chosen for solving the optimization problem and the definition of objective function, the solution could either converge to a local minimum or a global minimum. In a parameter identification problem, the first important step is to choose objective function in such a way that it contains sufficient information about all the parameters that are to be determined [58]. Once we have a well-defined objective function, the next step is to apply an appropriate optimization algorithm to minimize the objective function.

Deterministic optimization methods are based on computation of the gradient and Hessian and are particularly advantageous in reaching to a convergent solution faster than non-deterministic optimization methods [59]. Some examples of deterministic methods are Newton's method, Lavenberg-Marqardt method, line search approach and trust region reflective method. The main drawback of these methods is the possibility of converged solution being a local minimum rather than a global minimum. Stochastic search methods, simulated annealing, and smoothing methods are often used to find global minimum but are slow. These methods mainly differ in the criterion used for generating random search points. Homotopy is another popular optimization method, commonly used in solving non-linear problems, i.e, when the objective function is complicated. In homotopy, the optimization basically progresses by mapping a simple function with known global minimum to a more complication function. Vyasarayani et al.[60] developed a method to apply homotopy optimization in non-linear parameter identification of dynamic systems. They proposed that, for a physical system with mathematical model as follows:

$$\begin{aligned} \dot{x}_1 &= x_2 \\ \dot{x}_2 &= f(x_1, x_2, p, t) \end{aligned} \tag{2.1}$$

where, x_1, x_2 are the independent co-ordinates and p represents the parameter set. The objective function of this system can be modified by coupling the experimental data (x_{1e}) to the differential equations in its mathematical model as shown below:

$$\begin{aligned} \dot{x}_1 &= x_2 + \lambda K_1(x_{1e} - x_1) \\ \dot{x}_2 &= f(x_1, x_2, p, t) + \lambda K_2(x_{1e} - x_1) \end{aligned} \tag{2.2}$$

The differential equations were solved at every optimization step starting from λ=1, until it reaches 0, i.e the equations described in (2.2) morph back to those in (2.1), and finally a globally convergent solution is obtained. This method was successfully applied in the global parameter identification of a lithium-ion battery model [61], quasi-dimensional spark-ingnition engine model [62] and in the reduction of a vehicle multibody dynamic model [15].

2.4 Summary

In this chapter, different software available for multi-body vehicle dynamics modeling were introduced. Advantages and disadvantages associated with each software were discussed to identify the suitable software for developing the vehicle dynamics model concerned with this research work. Additionally, a brief literature review on classification of driving simulators and methods used for developing validated vehicle models for them were presented. It was found that most of the vehicle models were hand tuned for validation. This chapter also explored different standardized methods for obtaining suspension, tire, CG and inertia parameters and discussed various optimization algorithms available for parameter estimation from experimental data.

Chapter 3

Plug-in hybrid electric vehicle modeling

In this chapter, development of vehicle dynamics models for Toyota Prius PHEV 2015 is presented in detail. The first section presents a longitudinal dynamics model, which is developed using components from multibody, tire, and hydraulics libraries in MapleSim. The model inputs, outputs and important parameters necessary for the model simulation are discussed. In the second section, the driving simulator in Smart Hybrid and Electric Vehicle Systems (SHEVS) lab and ASM's generic vehicle dynamics model are presented. Also, modification of steering and brake sub-systems in the process of creation of a validated model for the driving simulator are described comprehensively in this section.

3.1 MapleSim model

MapleSim provides a multidomain modelling and simulation environment. Any model developed in MapleSim is suitable for HIL and Model in loop (MIL) tests due to its symbolic computation and optimized code generation capability. MapleSim has over 50 components in its multibody library such as rigid bodies, springs, dampers, connectors, and joints that can be dragged and dropped on to the worksheet to create our customized

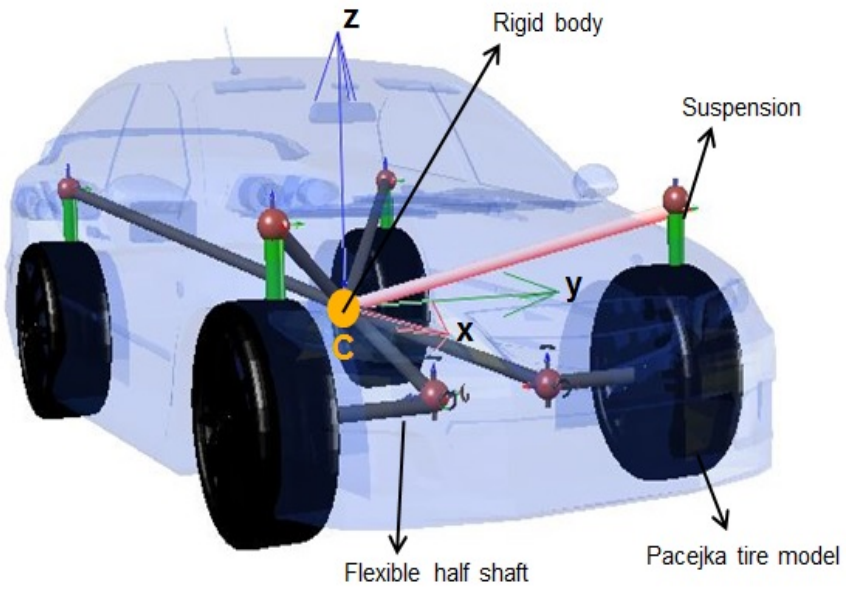

Figure 3.1: 3D representation of MapleSim model

multibody model. Hence, MapleSim is adopted for developing the longitudinal vehicle dynamics model of Toyota Prius, and its 3D representation is shown in Fig. 3.1.

The vehicle dynamics model of Prius has 18 DOF with 6DOF from chassis which is modelled as a rigid body, 4DOF from suspension, 4DOF from wheels and another 4DOF from the torsional deformation of two half shafts. The model's architecture consists of a rigid body connected to the tires through four suspensions. Torque input from the differential passes through the half shaft, whose one end is connected to the wheel and the other end is connected to the car body through universal joints. This configuration ensures that the drive train components are mounted on the chassis. Flexibility is introduced in the half shaft by modeling it as a torsional spring, damper and mass system. Pacejka's 2002 tire model is used in the vehicle dynamics model due to its suitability with wide range of operating conditions [63]. Suspensions are assumed to be linear and allow only vertical displacement in order to maintain the simplicity of the longitudinal vehicle dynamics model. A linear hydraulic brake module is added to each wheel to generate brake torque from the drivers brake pedal command. A simple on-off controller incorporated with hysteresis is

integrated with each brake to simulate the effect of anti-lock braking action during hard braking conditions.

3.1.1 Components used in modeling

Vehicle chassis

In this research, a rigid body is used to represent the vehicle chassis. In MapleSim, rigid body is described by its center of mass C and body fixed frame whose motion is tracked with respect to a fixed reference frame. It consists of mass M and inertia tensor I specified in terms of moments and products about C as shown in Fig. 3.1. A variant in rigid body component enables us to specify variable mass, where the mass of rigid body changes with an input signal connected to it. In this full vehicle model, location of this rigid body coincides with the location of CG. Considering that the vehicle starts from rest, all the necessary initial conditions for displacement and velocity are taken as zero. The rigid body is connected to other components at different locations through a rigid body frame that defines the position and orientation relative to the center of mass frame.

Suspension components

Suspension element connected to each tire is modeled using a prismatic joint. This joint allows relative translational motion in the vertical direction (along z-axis) between the two bodies that it connects. The motion of prismatic joint is governed by its spring constant K and damper constant C, thereby exhibiting linear characteristics. Although initial velocity of this component is given as zero, it is assumed to have some initial displacement resulting from the compression due to the weight of chassis.

Each prismatic joint is connected to the tire through a revolute joint that allows one rotational degree of freedom (along y-axis) after co-ordinate transformation. Spring stiffness and damping parameters of this revolute joint are assumed to be zero to simulate an ideal joint. The initial rotational speed of this joint is adjusted in accordance with the initial velocity given to the rigid body component described above.

Tire components

Each tire component consists of two sub-components: a standard tire body and a tire model. The tire body is described by a standard tire component that calculates the normal force and kinematic parameters such as slip angle, slip ratio, dynamic radii to determine force and moments on the tire. Important parameters that should be prescribed to a standard tire component are mass and inertia of tire, vertical stiffness, damping and unloaded tire radius. Effective rolling radius of tire during motion is calculated from its loaded radius. A tire model, which can be connected to the hub frame of standard tire component, takes the output information from tire body to calculate the forces and moments acting at the contact patch. MapleSim has a variety of tire models to serve this purpose such as linear, Fiala, Casplan, Pacejka, and user-defined. Pacejkas tire model, an empirical model whose parameters can be determined from the experimental data fitting, has been chosen in this work.

Brake module

On pressing a brake pedal, the force generated due to its application acts on a hydraulic master cylinder to generate hydraulic pressure. This pressure causes the movement of other cylinders inside of brake calipers. The calipers push the brake pads towards the rotor creating frictional force against the rotor surface. The wheel slows down under the action of a negative torque caused due to this frictional force. To simulate this process, MapleSim's hydraulics library, which comprises cylinders and circular pipes has been utilized. A '$tanh$' function that depends on the wheel speeds is introduced in the model of brake actuation force to nullify the magnitude of brake torque at near zero wheels speeds and avoid any discontinuities. Basically, the brake module in this vehicle model scales the position of brake pedal to obtain brake torque that can be applied on the tires.

Prius 2015 also consists of an anti-lock braking system which modifies the brake actuation force depending on the longitudinal slip generated at the tire contact patch. Hence, each brake module in the vehicle model is integrated with ABS to control the slip during harsh braking. ABS consists of an on-off controller that switches between the two Boolean states (true or false) based on the input slip ratio, a reference slip ratio and hysteresis. The reason behind including hysteresis in an on-off controller is to slow down the process

of switching between two states. A hydraulic lag modeled as a first-order transfer function is introduced, so that the pressure at the end of that line builds up through an integrator. The functioning of an ABS module depends on the reference and hysteresis values that rely on maximum and minimum slip allowed for the vehicle.

Half shaft components

Half shaft is modeled as a torsional spring, damper, mass system (1DOF) whose main parameters are torsional stiffness, damping and inertia of half shaft. An ideal prismatic joint (1DOF) has been added to this system to allow the displacement of wheel in lateral direction. The connection between half-shaft and tire is provided by an ideal universal joint that can be considered as a composite joint comprising of two revolute joints.

3.1.2 Model inputs and outputs

Figure 3.2: Inputs and outputs of the MapleSim model

The output torque from the power-split planetary gear set acts as an input to the vehicle dynamics model. This input torque is magnified as it passes through final drive which is modelled as an ideal gear component with gear ratio r. Brake pedal position is another input to the model through which brake torque is applied at each wheel. The output velocity of the vehicle is used to generate the effect of aerodynamic drag force along

longitudinal direction. This drag force is assumed to act at the center of gravity of the vehicle by attaching an applied world force component to the rigid body mass. Other important outputs from this model are wheel speeds, longitudinal acceleration, jerk and slip.

3.2 Driving simulator vehicle dynamics model

The driving simulator in smart hybrid electric vehicle systems (SHEVS) lab is built at a lower cost with all the necessary features specific to its usage. The two main purposes for which this simulator is intended are: (1) Driving data collection through virtual driving, (2) Controller performance evaluation and rapid control prototyping. It is a PC based simulator that provides 135°, fixed seat base, gear shifter and a steering wheel with self-centering feature and maximum of 900° rotation. Fig. 3.3 shows the driving simulator in SHEVS lab.

Figure 3.3: Driving simulator in SHEVS lab

It can perform simulations in real-time through dSPACE's DS 1006 processor, which

is designed for calculating complex, detailed simulation models that require enormous computing power. Any developed controller algorithm can be deployed on MicroAutobox hardware, that operates just like an ECU and performs fast function prototyping. MicroAutobox monitors and interacts with the DS 1006 real-time processor to send and receive feedback signals. The vehicle model, visualization and traffic simulation in this driving simulator are provided by the dSPACE's ASM simulation package, which follows an 'open model concept' [64]. This implies that the simulation models in this package are Simulink blocks and can easily be altered to develop dedicated models specific to this project. The main software components of ASM chosen of this simulator are ASM vehicle dynamics, ASM model desk, ASM motion desk, ASM control desk and ASM traffic simulator. All these software and hardware interface with each other to provide real-time virtual simulation.

ASM vehicle dynamics model is a very detailed multibody system that consists of different subsystems of a vehicle such as chassis, suspensions, wheels, brakes and steering system. The model receives inputs from the powertrain, driver and environment which include signals such as half shaft torques, road friction coefficient, steering wheel angle, brake pedal position, wind velocity and initial conditions of the vehicle. The most important model outputs are the signals that describe the motion of the vehicle such as longitudinal and lateral velocity, longitudinal and lateral acceleration and yaw rate.

This package comes with the complete implementation of two tire models: Pacejka 2002 and TMEasy. The former has been chosen for vehicle modeling to maintain consistency with previously described MapleSim model. The tire model is capable of simulating first order transient tire dynamics in lateral, longitudinal and vertical directions. Dynamic radius of the tire that varies significantly with tire load is calculated based on an empirical Magic Formula (MF) type formula relating the nominal tire load, vertical tire stiffness and unloaded radius. The behavior of tire on different road surface conditions such as dry, wet, damp and icy is simulated by switching the friction coefficients of the tire model online. Major changes are not made to this module except that the dynamic radius is calculated using loaded radius as shown in equation (3.1) to avoid the parameters required for MF type empirical formula.

$$r_{dyn} = r_{loaded} = r_{unloaded} - z_{wheel-disp} \tag{3.1}$$

A linear or a non-linear (physical master cylinder) model can be used to simulate the brake hydraulics in ASM vehicle dynamics model. Linear model is based on the maximum cylinder pressure, whereas, non-linear model implements the action of a brake booster and uses look-up table based brake force map to obtain brake torque on each wheel. Due to unavailability of data required for generating maps or parameterizing a non-linear model, the simple linear model has been chosen for modeling. However, this model requires further implementation of ABS. So, the linear brake module with anti-lock braking system that has been developed previously for MapleSim vehicle dynamics model has been utilized. The MapleSim model's brake module is converted to Simulink S-function and imported into ASM model to replace the existing brake hydraulics module. Also, the brake torque associated with regeneration from motor is applied directly through half-shaft torque input.

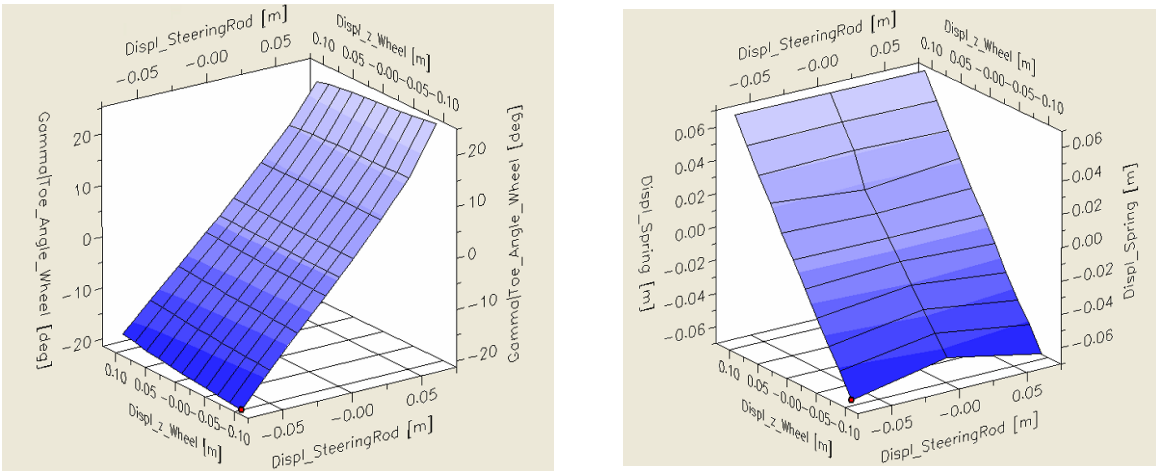

Figure 3.4: 3D Maps in ASM for simulating suspension kinematics

The generic steering model in ASM simulates a front wheel rack and pinion steering system. It accepts steering wheel angle and self-aligning torques from front tires as inputs and gives steering rod displacement as an output. The table based suspension system makes use of this output from steering system, along with the vertical displacements of the wheels to simulate suspension kinematics. It consists of maps as shown in Fig. 3.4 for the

displacement and orientation of the wheel, displacement of spring, damper and stabilizer bar. Obtaining such maps specific to Prius requires a standardized test procedure called Kinematics and Compliance testing, which is inaccessible and expensive as discussed in Chapter 2. Consequently, the steering model has been modified to output the turn angle (toe) of the wheel obtained by dividing the steering wheel angle with the steering ratio. This steering ratio for Prius 2015 can be estimated from the experimental data collected through on-road testing, which will be discussed in Chapter 6. Also, the influence of steering rod displacement on the camber and caster of wheel, and the spring and damper of the suspension are considered as secondary effects and are neglected in this study. To determine the forces in the suspension, ASM model uses another linear map based on the displacements of spring and damper obtained from suspension kinematics. The slope of this linear map can be adjusted based on the suspension stiffness and damping coefficients determined through parameter identification, which will be discussed in Chapter 6.

The aerodynamic forces and moments in this model are calculated based on the incident angle of the wind through non-linear maps. In this research, only influence of longitudinal aerodynamic drag force at zero incidence angles to the vehicle is considered and the forces and torques in remaining directions are nullified. Ultimately, the vehicle movement is described by the net force and torque acting at the center of gravity of vehicle whose location has to be pre-defined before the simulation. The outputs from all the subsystems are combined to formulate a 10×1 force matrix (F) that includes forces from tires, suspension, aerodynamics, and other external effects and a 10×10 mass matrix (M) that includes mass and inertia of the vehicle and wheel. These matrices are used to calculate the translational and rotational speeds of the vehicle body and also the vertical displacements of each tire by performing discrete integration of the accelerations obtained from equation (3.2). This implies that ASM model is a 10DOF system with 6DOF from vehicle body and 4DOF from vertical displacements of tires.

$$[a]_{10\times1} = [M]^{-1}_{10\times10}[F]_{10\times1} \tag{3.2}$$

The parameters required for the online and offline simulation of this ASM vehicle dynamics model can be prescribed and modified using ASM ModelDesk. It provides parameter

GUIs with demonstration of each component. Table based parameters can be visualized as 3D maps as shown in Fig. 3.4. ModelDesk also consists of a road generator that is used for defining the virtual road based on a reference line. Road features such as heights, inclinations, lanes and surfaces can be set to the generated road profile based on requirements. After generating a road, maneuver editor is used to define the road path along which vehicle is supposed to move.

3.3 Summary

This Chapter presented the development of vehicle dynamics models of Prius in MapleSim and ASM software. The former was a reduced multibody model, developed by utilizing the components in MapleSim libraries, while the later was modified based on the detailed generic vehicle dynamics model in ASM. MapleSim model was only a longitudinal dynamics model with torque and brake pedal position as inputs, whereas ASM model was capable of performing handling maneuvers by taking steering angle as an additional input. Parameters necessary for the simulation of each model were also discussed. Methods for obtaining these parameters and validation of these models is discussed in the following chapters.

Chapter 4

Experimental setup

This chapter presents the test vehicle and a detailed description of the measurement sensors used for the data collection. The vehicle is tested in different facilities which include Toyota Motor Manufacturing Canada (TMMC) test track, Green and Intelligent Automotive (GAIA) lab and Multimatic's 4-Post rig. Various test scenarios such as acceleration and braking, double lane change, step steer, and speed bump maneuvers are performed on the track to excite the vehicle longitudinally, laterally and vertically. These tests are necessary to validate the vehicle dynamics models presented in Chapter 3.

4.1 Measurement sensors

The test vehicle chosen for this study is Toyota Prius Plug-in Hybrid 2015 with front engine, two axle and front wheel drive (FWD) layout. Vehicle is instrumented with multiple external sensors to measure the response of vehicle body and tires while driving. The system of sensors include vehicle measurement system (VMS), global positioning system (GPS) and inertial measurement system (IMU). Signals from VMS, GPS, IMU and vehicle Controller Area Network (CAN) are recorded and integrated with the help of a CAN integration device from 'Vector Informatik GmbH'. This device facilitates all the collected signals to have a common time stamp. The system architecture for integrating the signals from the three devices using the Vector is shown in Fig. 4.1.

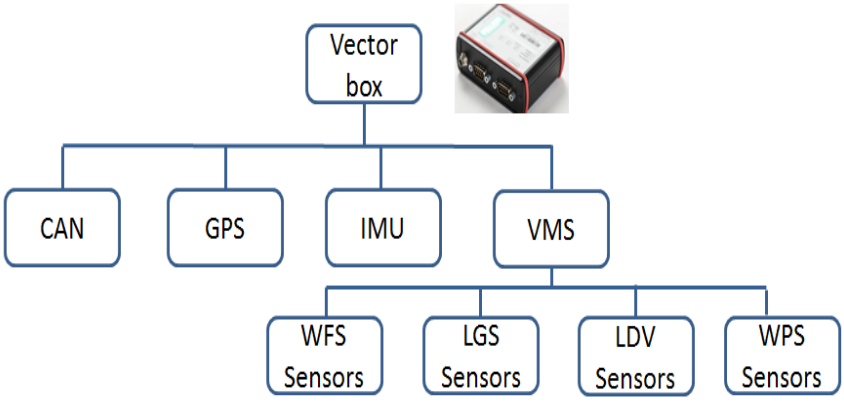

Figure 4.1: System architecture for data collection

Vehicle measurement system (VMS): VMS, a product of A&D Tech, acquires synchronized vehicle dynamics data from on-road testing by utilizing combination of embedded controllers and high accuracy sensors. Sensor attachments are modular, which facilitates the usage of required sensors specific to the application. Following are the sensors of VMS that are installed on the vehicle as shown in Fig. 4.2 for collecting test data in this research work.

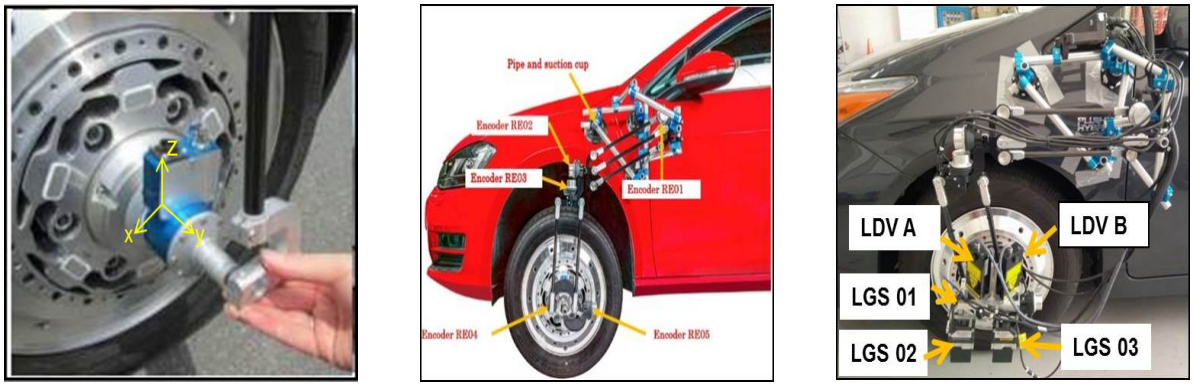

(a) (b) (c)

Figure 4.2: Vehicle measurement system: (a) WFS sensors, (b) WPS sensors, and (C) LGS sensors

Wheel force sensor (WFS): It measures forces (F_x, F_y, F_z) and moments (M_x, M_y, M_z) acting on the wheel hub under dynamic conditions in all 6-axis. It uses force detection bridges that are composed of shear beams and shear strain gauges that ensure high level of robustness in the measurements. A rotary encoder is installed inside the bearing to measure rotational speed of the tire. Force measured at the wheel hub is adjusted using Newton's laws to obtain the force generated at the tire contact patch.

Laser ground sensors (LGS): This set of sensors are attached to the wheel hub and are a combination of three laser distance sensors (LDS) and two laser Doppler velocimeters (LDVs). The LDSs measure the dynamic change in the wheel height during driving through laser reflection. LDVs measure ground speed of the tire in longitudinal and vertical direction along with tire rotation speed around lateral axis. LGS sensors give additional information about dynamic tire radius, slip angle, camber angle, pitch angle, roll angle of that specific tire to which they are attached after performing internal calculations.

Wheel position sensor (WPS): This consists of five individual encoders that are used to measure wheel movement with respect to a reference point on the vehicle body. One end of this whole sensor set is attached to the wheel hub while the other end is attached to vehicle body through suction cups. The data collected from this sensor includes relative displacement and rotation about longitudinal, lateral and vertical axis of wheel to which they are attached. The data from these sensors is important in understanding the suspension kinematics of the vehicle.

Inertial measurement unit (IMU): The IMU used for testing is a product of Racelogic. It provides accurate measurements of pitch, roll and yaw rate using three rate gyroscopes along with longitudinal, lateral and vertical accelerations via three accelerometers. The IMU roof mount with magnetic base allows the IMU to be placed directly on the vehicle roof and protects it from external environment. It is integrated with global position sensor (GPS) antenna to ensure that the data from GPS and IMU comes from the same point. This GPS antenna tracks satellite to give additional information about position and velocity of the vehicle. The IMU + GPS antenna unit is mounted on vehicle roof in such a way that GPS antenna has clear view of the sky for accurate measurements.

There is also a physical switch on the brake pedal known as brake pedal trigger that

gives precise measurement of brake pedal application.

Controlled area network (CAN bus): The data from vehicle CAN bus gives information from the internal sensors and ECUs of the vehicle. Signals collected from CAN bus include steering wheel angle, brake pedal position, vehicle speed and acceleration, motor/generator speed and torque, and engine speed signals.

4.2 Test facilities

TMMC test track:

(a) (b)

Figure 4.3: TMMC test track: (a) Prius with external instrumentation, and (b) Aerial view of TMMC test track

Detailed tests were conducted at Toyota Motor Manufacturing Canada (TMMC) test track shown in Fig. 4.3 with the data coming from VMS, GPS, IMU sensors and CAN bus described above. Before starting the actual testing, calibration tests were carried out to make sure that all the sensors display data in the expected range. Specific tests were designed to excite specific set of vehicle parameters. Straight line driving maneuvers provide necessary information for characterizing the longitudinal vehicle dynamics of the vehicle. These tests included hard acceleration and hard braking, hard acceleration, cruise

and normal braking, coast down and driving over a speed bump. During coast down tests, wind speed was also recorded from the TMMC weather station. Additionally, some lateral maneuvers were performed to excite lateral dynamics of the vehicle. These tests included double lane change maneuvers, steady state cornering tests, step steer maneuvers and step steer with braking maneuvers. Due to unavailability of engine torque data from CAN bus, few tests were performed especially in EV mode of the vehicle to check for the consistency of WFS measurements with CAN bus signals.

Green and Intelligent Automotive (GAIA) lab:

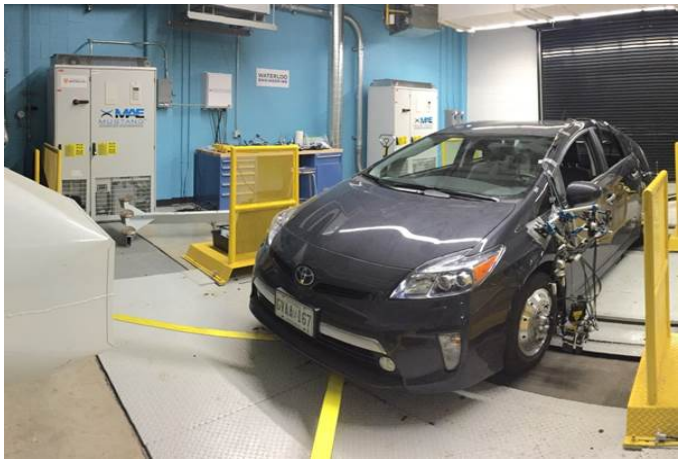

Figure 4.4: Prius on rolling dynamometer in GAIA lab

Due to unsuitable weather conditions, it was not always possible to drive the vehicle with multiple external sensors on an open test track. In such cases, Mustang's chassis dynamometer at GAIA lab shown in Fig. 4.4 was utilized to execute indoor vehicle testing. Chassis dynamometer consists of two mechanically-linked rollers rotating at same speed to simulate a dry, flat road condition. The speed of the large cooling fan situated in front of the dynamometer varies with the speed of the vehicle to ensure prolonged testing. Before starting the test, the dynamometer's software was loaded with weight, maximum power and torque data of the Prius, from its in-built database of vehicles. After few initial tests, the torque data obtained from WFS and CAN was cross-validated against the dynamometer measurements to ensure consistency. Acceleration and braking tests were performed in EV

and Hybrid modes of Prius to collect data necessary for parameter identification. It was observed that the dynamometer testing is unsuitable for hard acceleration, hard braking and maneuvers with non-zero steering input.

Multimatic's 4-Post test rig:

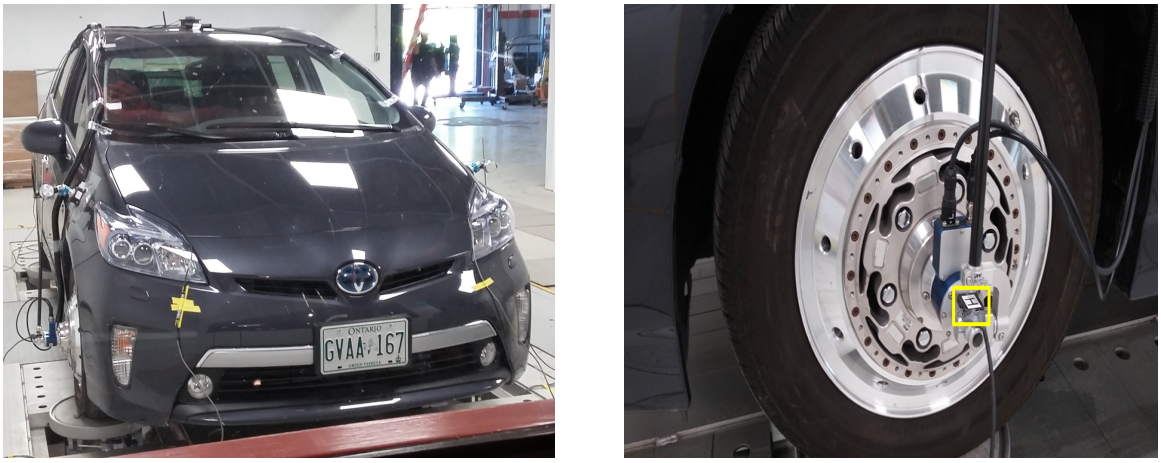

(a) (b)

Figure 4.5: 4-Post test rig: (a) Prius on 4-Post rig and (b) Accelerometer attached to the wheel hub

At this facility, Prius was mounted on four rams that transmit vertical excitations to the vehicle through tire contact patch. Before testing, accelerometers were attached to the wheel hub and sprung mass of Prius as shown in Fig. 4.5. During the test, input excitation given to vehicle was a constant amplitude sinusoidal wave with frequency sweep ranging from 0 to 30 Hz. Load cells at the tire contact patch and accelerometers provide necessary information to determine the characteristics of sprung and unsprung masses. Data collected from these sensors was utilized by 4-Post rig engineers to perform frequency domain analysis on a full vehicle model. Parameters obtained from this analysis include suspension stiffness and damping at front and rear end, tire vertical stiffness and pitch inertia of the vehicle. The test procedures used at this facility were developed and improved over years of research. Hence, parameters from this testing are considered to be accurate and are laid as a basis to determine the accuracy of parameters obtained from the track

tests, which will be discussed in Chapter 5.

4.3 Summary

In this chapter, experimental set up and test facilities were presented. The system architecture for data integration and each measurement sensor's location and function was described in detail. This chapter also introduced different test facilities such as TMMC proving ground, GAIA lab and Multimatic's 4-Post rig, which were utilized during vehicle testing. Tests performed, procedure followed and any limitations associated with each test facility were discussed briefly.

Chapter 5

Parameter estimation

The vehicle dynamics models in MapleSim and ASM vehicle dynamics software have to be specified with accurate parameters of Toyota Prius PHEV 2015 for vehicle dynamics simulation. Few parameters such as wheelbase and front and rear track widths can be obtained directly from physical measurements. But, these are insufficient to describe the behaviour of the vehicle under the influence of several external forces. More experimental data and mathematical calculations are necessary to compute important vehicle parameters such as frontal area, center of gravity height, rolling resistance coefficient, half shaft parameters, suspension parameters and tire parameters. In this chapter, the data from on-road and dynamometer testing of the Prius equipped with the instrumentation described in Chapter 4 is used in the process of parameter estimation. The data collected from specific maneuvers is processed to estimate specific sets of parameters. For this purpose, the equations of motion of the vehicle containing the specific parameters to be determined are chosen and solved, instead of using a complete vehicle dynamics model that has many other unknown parameters. A MATLAB/Simulink based non-linear least squares method is chosen for minimizing the objective function of each parameter identification problem.

General forces acting on a vehicle in longitudinal motion are described as shown in Fig. (5.1). Neglecting the relative motion between wheels and chassis, the dynamic equation for the longitudinal motion of the vehicle is expressed as:

$$M\ddot{x} = F_{xf} + F_{xr} - F_{rf} - F_{rr} - F_d \tag{5.1}$$

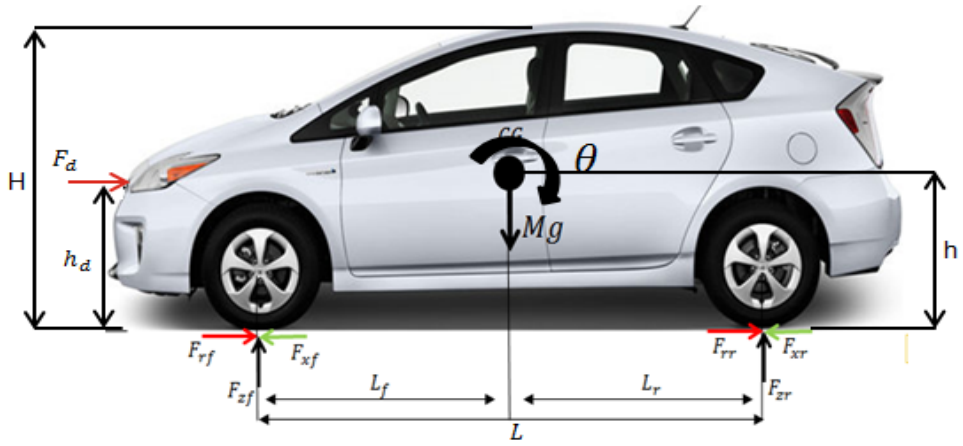

Figure 5.1: Forces acting in longitudinal direction on Prius

where, M represents the total mass of the vehicle. F_{xf}, F_{xr} are the longitudinal traction/braking forces acting on the front and rear wheel. F_{rf}, F_{rr} are the rolling resistance forces on the front and rear wheels. F_d is the aerodynamic drag force on the vehicle acting at the center of pressure (CP), which is located at a height of h_d from the ground. Also, F_{zf} is the sum of normal forces on the front left and right wheels and F_{zr} is the sum of normal forces on the rear left and right wheels. L is the wheel base of the vehicle. The longitudinal distance of center of gravity (CG) from front and rear wheels are L_f and L_r respectively, while the vertical distance of CG from ground is represented by h.

Mass of the vehicle (M) is calculated by adding the normal loads acting on all four tires. These normal load measurements are obtained from wheel force sensors while the vehicle is resting on a levelled surface. Also, the weight contribution from all the sensors equipped on the vehicle is deducted from the readings to obtain the true vehicle mass.

(a) (b)

Figure 5.2: Frontal area: (a) Frontal image of Prius and (b) Processed frontal image of Prius to black and white

5.1 Frontal area

According to the U.S. Environmental Protection Agency (EPA), frontal area of a vehicle is defined as, "the area of the orthogonal projection of the vehicle on a plane perpendicular to the longitudinal axis of the vehicle". Frontal area depends on the exterior design of a vehicle and is an important parameter in deciding the amount of aerodynamic drag experienced by the vehicle during motion. It indirectly influences the fuel consumption of the vehicle and hence has to be estimated accurately.

In this research work, frontal area is estimated using image processing techniques. At first, frontal image of Prius PHEV was processed to fill the region of the car with black and the back ground with white color [65]. Then 'im2bw' function in MATLAB is used to convert the grey scale image to binary image. The grey scale image's darker pixels are replaced by 0 and lighter pixels are replaced by 1 in the final binary image as shown in Fig 5.2b. Percentage of area with black pixels is determined and scaled back to the actual size of the Prius. From this technique, frontal area of Prius is estimated as $2.19\,\mathrm{m}^2$, which is 84.2% of the total area of the box ($2.60\,\mathrm{m}^2$).

5.2 Rolling resistance coefficient

Tire rolling resistance coefficient (f_{rr}) is obtained from the data acquired during vehicle coast down testing on a flat road. During this test, vehicle is accelerated to a high speed and is allowed to decelerate to a low speed without any inputs from accelerator or brake pedal. Also, after reaching maximum speed, the gear is shifted to neutral in order to mitigate the effect of drivetrain drag on vehicle coasting. Hence, the aerodynamic drag and rolling resistance force are the only forces contributing to the deceleration of the vehicle. Assuming the vehicle as a rigid body, the equation governing its longitudinal dynamics motion during coast down is expressed as:

$$M\ddot{x} = -\frac{1}{2}\rho A_f C_d (V + V_w)^2 - f_{rr} M g \tag{5.2}$$

where, A_f and C_d are the frontal area and drag coefficient of the vehicle respectively. V and V_w are the components of velocity of the vehicle and wind in longitudinal directional respectively. The first term in left hand side of equation (5.2) represents aerodynamic drag force, while the second term represents rolling resistance force acting on the vehicle.

To eliminate the effect of fluctuating wind speeds, tests were conducted on a calm day and six runs of coast down tests were performed with and against the wind. In each test, the vehicle is accelerated to a speed of 70km/hr and is coasted to a speed of 25km/hr under the action of road load forces. The non-linear differential equation (5.2) is solved using MATLAB's ODE 45 and also optimized simultaneously for f_{rr} through least squares minimization of velocity errors. Coefficient of drag of Prius PHEV 2015 was chosen to be 0.25 [66] in the estimation process. Fig. 5.3a shows the simulated and experimental velocities after the estimation of f_{rr} in a specific run. The average coefficient of rolling resistance is obtained as 0.012 from the results of all runs shown in Fig. 5.3b.

5.3 Location of center of gravity

In this work, CG location is identified by exciting the longitudinal and pitch dynamics of the vehicle through rapid acceleration and hard braking tests, thereby avoiding the need

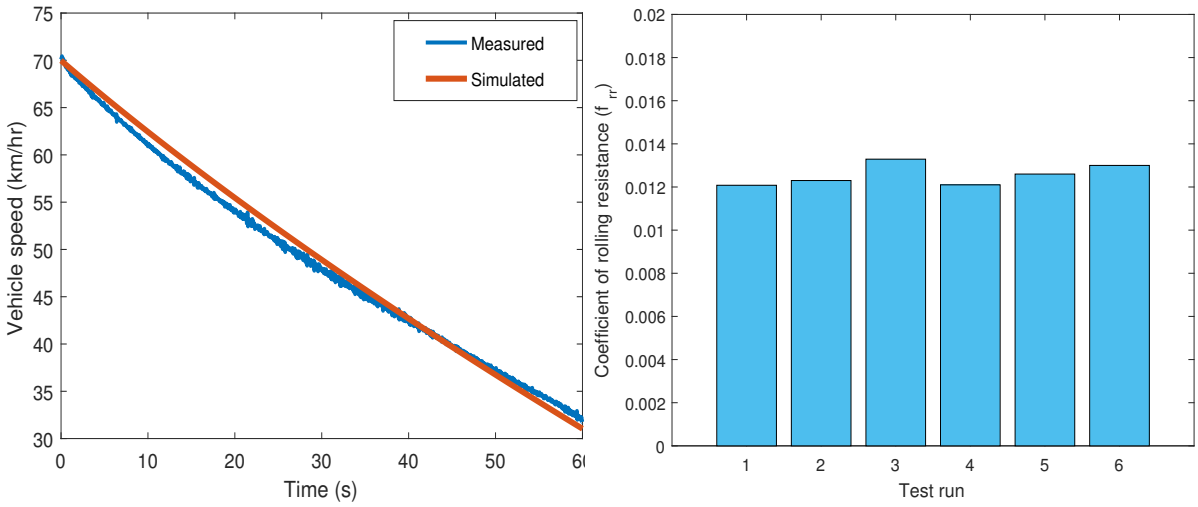

(a) (b)

Figure 5.3: Coast down test: (a) Vehicle speed vs time to estimate f_{rr} and (b) Bar graph of rolling resistance coefficients obtained for six different runs

for dangerous lateral, yaw or roll motions. The redistributed vertical loads on tires during a hard acceleration/braking maneuver contain the major information necessary to determine the location of CG of the vehicle. The equation governing the pitch motion of the vehicle is expressed as:

$$I_y\ddot{\theta} = -F_{zf}L_f + F_{zr}L_r - Ma_{xCG}h \tag{5.3}$$

where, I_y is the pitch inertia of the vehicle. The equation (5.3) is re-arranged to obtain vertical force on the front wheels as:

$$F_{zf} = \frac{MgL_r}{L} - \frac{Mha_{xCG}}{L} - \frac{I_y\ddot{\theta}}{L} \tag{5.4}$$

Also, due to considerable amount of pitching during a hard acceleration and braking maneuver, longitudinal acceleration at the center of gravity of the vehicle is slightly different from the longitudinal acceleration measured by GPS sensor (a_{xGPS}), located at the top

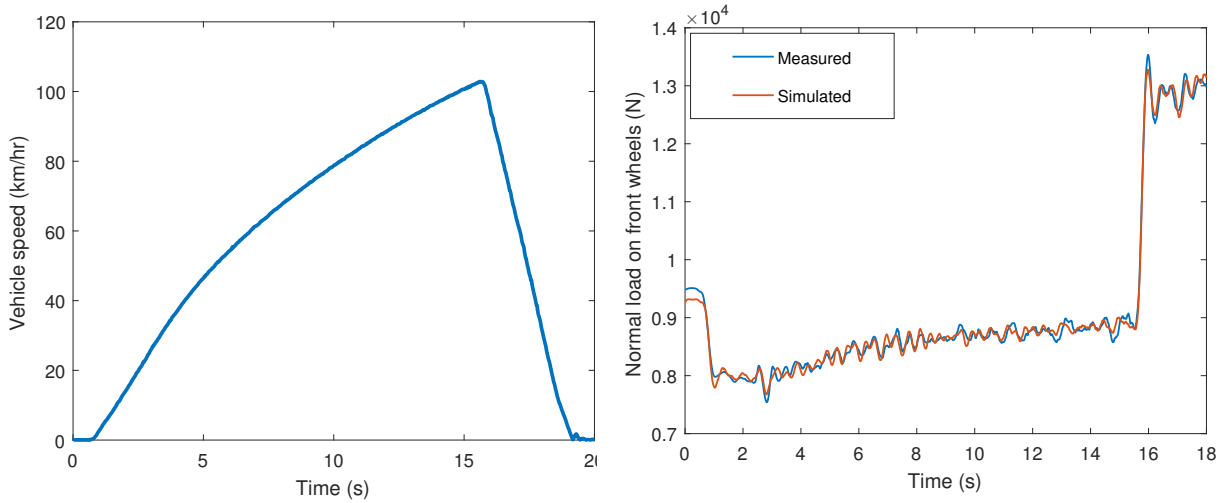

(a) (b)

Figure 5.4: Acceleration and braking maneuver: (a) Vehicle velocity and (b) Simulated normal force on front wheels compared against the measurements from WFS

of the vehicle. Hence, using acceleration transformation equation for a rigid body and neglecting the terms associated with insignificant yaw and roll rates, a_{xCG} is obtained as:

$$a_{xCG} = a_{xGPS} + \ddot{\theta}(r_{CG} - r_{GPS})_z \tag{5.5}$$

where, H is the height at which GPS is mounted from the ground. After substituting equation (5.5) into (5.4), we have:

$$F_{zf} = \frac{MgL_r}{L} - \frac{Mh_{CG}(a_{xCG} + \ddot{\theta}(h - H))}{L} - \frac{I_y\ddot{\theta}}{L} \tag{5.6}$$

Pitch acceleration ($\ddot{\theta}$) is obtained by taking the derivative of pitch rate ($\dot{\theta}$) measured by the GPS. Also, load on the front wheels is measured by wheel force sensors. Parameters h, L_r and I_y are estimated by the non-linear least squares minimization of the difference between experimental and simulated values of F_{zf}.

Fig. 5.4b shows the experimental and simulated data for F_{zf} while accelerating the vehicle from 0 to 100 km/hr and braking from 100 to 0 km/hr. Contribution of road grade on F_{zf} is neglected during estimation as the tests are done on a flat road. Table 5.1 shows the estimated values of CG height, longitudinal location of CG and pitch inertia for three different acceleration and braking maneuvers. Mean values of these readings will be used in the simulation of full vehicle dynamics model.

Test No.	**h(m)**	**L_r(m)**	**I_y(kgm^2)**
1	0.60	1.46	2958
2	0.60	1.46	3001
3	0.61	1.46	2760
Mean	0.60	1.46	2888

Table 5.1: CG height, CG longitudinal location from rear tires and pitch inertia for different test runs

5.4 Suspension and steering parameters

Suspension parameters: Prius PHEV 2015 consists of an independent McPherson strut suspension in the front and a torsion beam suspension in the rear. However, during vehicle modeling phase, suspensions are assumed as vertical linear spring and damper elements at each wheel. The main reason behind this assumption is that it best fits when front/rear load transfer is taken into consideration, i.e, during acceleration and braking situations. Also, linearity in suspension components facilitates us to gain more insight about the working of model. Besides these assumptions, suspension elements are also considered to be symmetric about longitudinal axis. Consequently, for parameter identification, the full vehicle dynamics model is reduced to a 4 degree of freedom half car model. Vertical stiffness and damping coefficients of suspensions and tires are identified through vertical dynamics analysis of the half car model as shown in Fig. 5.5. This model is represented by unsprung masses of front and rear wheels, m_{tf} and m_{tr}, and sprung mass of the vehicle body M_s. I_s is the pitch inertia of sprung mass, which is obtained by subtracting the

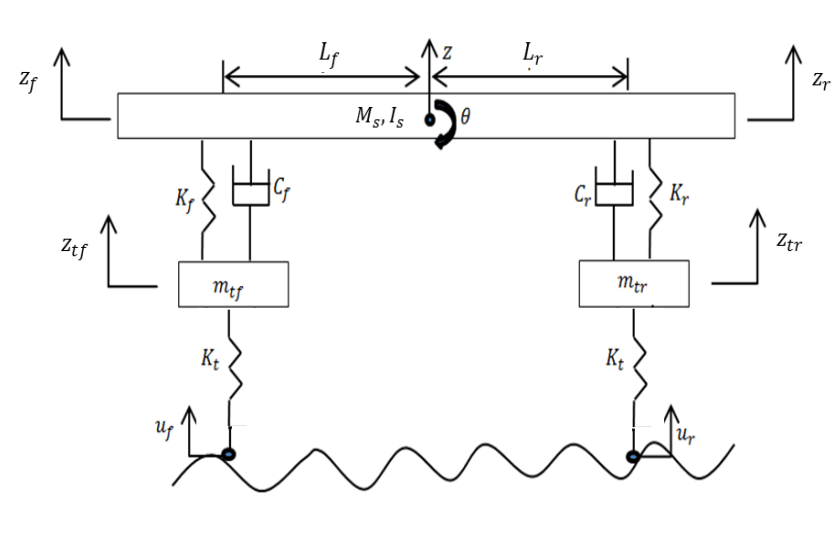

Figure 5.5: Half car suspension model

pitch inertia (I_y) of the vehicle from the inertia of unsprung mass about CG. Suspension elements are characterized by stiffness coefficients K_f and K_r and damping coefficient C_f and C_r. Elasticity in the tire is described by a spring with stiffness coefficient K_t. Damping of the tire is neglected in the vertical dynamics analysis as it is insignificant compared to the damping of suspension. The equations of motion of all the masses in half car model when subjected to a vertical excitation are expressed as:

$$\begin{aligned}
M_s\ddot{z} &= -K_f(z_f - z_{tf}) - K_r(z_r - z_{tr}) - C_f(\dot{z}_f - \dot{z}_{tf}) - C_r(\dot{z}_r - \dot{z}_{tr}) \\
I_s\ddot{\theta} &= L_f(K_f(z_f - z_{tf}) + C_f(\dot{z}_f - \dot{z}_{tf})) - L_r(K_f(z_r - z_{tr}) + C_r(\dot{z}_r - \dot{z}_{tr})) \\
m_{tf}\ddot{z}_{tf} &= K_f(z_f - z_{tf}) + C_r(\dot{z}_f - \dot{z}_{tf}) - K_t(z_{tf} - u_f) \\
m_{tr}\ddot{z}_{tr} &= K_r(z_r - z_{tr}) + C_r(\dot{z}_r - \dot{z}_{tr}) - K_t(z_{tr} - u_r) \\
z_f &= z + L_f\cos\theta \quad \text{and} \quad z_r = z + L_r\cos\theta
\end{aligned} \tag{5.7}$$

During the test, the vehicle is driven over a speed bump of known geometry to excite pitch and heave motions. z, z_{ft} and z_{rt} are the vertical displacements of individual masses from the vehicle's static equilibrium position and θ is the pitch angle of the sprung mass. Finally, u_f and u_r are the road profile inputs to the half car model.

$$u_{f,r} = \begin{cases} 0, & \text{if } t < \frac{D_{f,r}}{v} \\ \frac{A}{2}\Big(1 - \cos\big(\frac{2\pi}{\lambda} D_{f,r}(t)\big)\Big), & \text{if } D_{f,r} \leq t \leq \frac{D_{f,r}+\lambda}{v} \\ 0, & \text{if } t > \frac{D_{f,r}+\lambda}{v} \end{cases} \tag{5.8}$$

$D_{f,r}$ is the horizontal distance recorded by LGS sensors at the front and rear wheels before encountering the speed bump of height A and width λ. Normal load on the front and rear tires is given by:

$$\begin{aligned} F_{zf} &= (M_{sf} + m_{tf})g - K_t(z_{ft} - u_f) \\ F_{zr} &= (M_{sr} + m_{tr})g - K_t(z_{rt} - u_r) \end{aligned} \tag{5.9}$$

where, M_{sf} and M_{sr} are the sprung masses at the front and rear. The first term on the left hand side of equation (5.9) represents the load on the tire due to static weight (at t=0 s), while the second term represents the dynamic tire load. The objective function to be minimized is shown in equation (5.10) with K_f, K_r, C_f, C_r and K_t as the parameters to be estimated.

$$\begin{aligned} J_1 &= F^*_{zf} - (M_{sf} + m_{tf})g + K_t(z_{ft} - u_f) \\ J_2 &= F^*_{zr} - (M_{sr} + m_{tr})g + K_t(z_{rt} - u_r) \\ J_3 &= \dot{\theta}^* - \dot{\theta} \\ J &= \int_0^t \big((w_1 J_1)^2 + (w_2 J_2)^2 + (w_3 J_3)^2\big) dt \\ &\text{Objective function:} \quad \min J \end{aligned} \tag{5.10}$$

where, F^*_{zf}, F^*_{zr} are the normal loads measured by WFS sensors on front and rear tires. $\dot{\theta}^*$ is the pitch rate measured by IMU sensor. J_1, J_2, and J_3 are normalized by their respective experimental values at the start of bump (t=8 s) through w_1, w_2, and w_3. The above objective function is minimized using three different optimization methods: trust-region reflective algorithm, homotopy, and genetic algorithm. Trust region reflective algorithm, which was applied to identify parameters in previous sections, is a local optimization method. As the parameter identification problem in this section has 5 parameters, there is a high

possibility that the objective function minimized using trust region reflective algorithm converges to a local minimum. Hence, homotopy, a computationally efficient global optimization technique is also investigated to estimate these 5 parameters. According to the procedure proposed by Vyasarayani et al.[60], the governing differential equation relating to the pitch motion is modified as follows:

$$I_s\ddot{\theta} = L_f(K_f(z_f - z_{tf}) + C_f(\dot{z}_f - \dot{z}_{tf})) - L_r(K_f(z_r - z_{tr}) + C_r(\dot{z}_r - \dot{z}_{tr})) + \lambda K(\dot{\theta}^* - \dot{\theta}) \quad (5.11)$$

The equation (5.11) is coupled with the experimental data of pitch rate, as the other available data is either coupled with the parameters to be estimated or consists of relative measurements. In this optimization problem, $\delta\lambda = 0.1$ and $K = 20$. Optimization starts with $\lambda = 1$, and is decreased in steps of $\delta\lambda$ until it reaches 0. It is observed that the parameters estimated from homotopy optimization method are similar to those estimated from the trust region reflective algorithm method. To further ensure better confidence in results, genetic algorithm, a stochastic global optimization method was chosen to estimate the parameters. The values obtained from homotopy and trust region reflective algorithm are compared against those obtained from the genetic algorithm in Table 5.2. The values from genetic algorithm obtained after 150 iterations (computation time: 150min) are very close to those from homotopy optimization (computation time: 10min).

The parameters from speed bump testing showed a deviation of $\pm$ 10% from the results of 4-Post testing (Multimatic model parameters). There are mainly two reasons for these differences. The first is that, in 4-Post testing, vehicle tires were resting on rams that provide vertical excitation, whereas in a speed bump test, tires were rolling while travelling over the bump. The rolling motion could alter the stiffness of tires, which in the end affects the estimates of suspension parameters. The other reason is that, Multimatic's half car model has an additional installation stiffness modeled in between vehicle body and suspension. This additional stiffness is absent in the half car model used in this research. Fig. 5.6 shows the experimental and simulated values of load on front and rear wheels measured while the vehicle is traveling over a speed bump of height 0.07 m and width 0.48 m at a constant velocity of 15 km/hr.

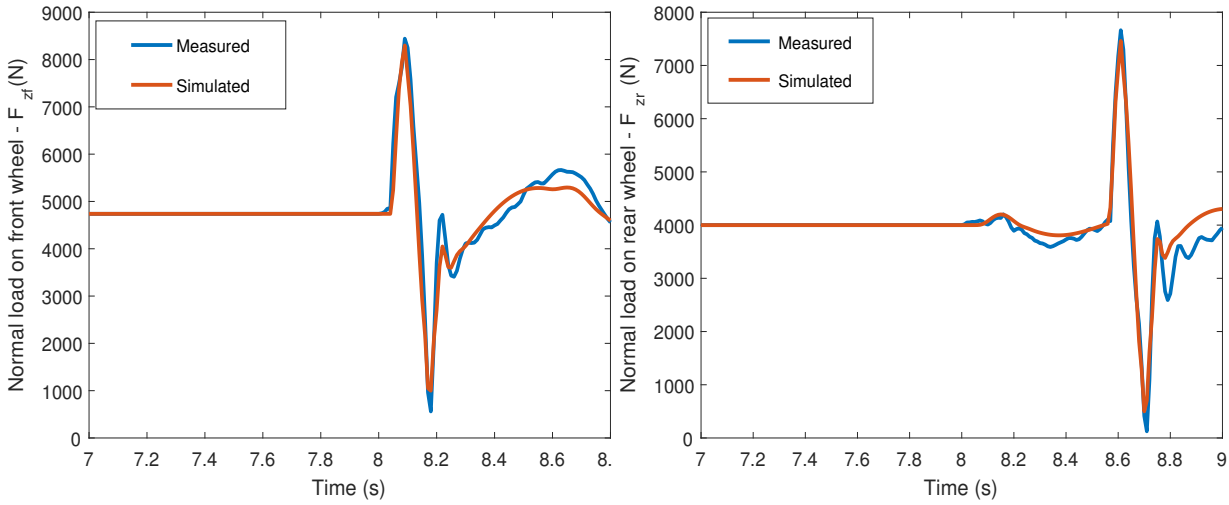

(a) (b)

Figure 5.6: Speed bump test: (a) Normal force on the front wheels and (b) Normal force on the rear wheels

Parameter	**Homotopy and Trust-region**	**Genetic algorithm**	**4-Post testing**	**Units**
$\mathbf{K_f}$	31052	30652	29000	N/m
$\mathbf{C_f}$	2019	2024	2300	Ns/m
$\mathbf{K_r}$	24321	23530	25000	N/m
$\mathbf{C_r}$	2088	2092	1600	Ns/m
$\mathbf{K_t}$	281235	274428	265000	N/m
Objective func.(J)	4.35	4.36	–	–

Table 5.2: Suspension parameters obtained from speed bump testing and 4-Post testing

Steering ratio: Steering ratio is defined as the ratio of the rotation of steering wheel to the toe-in angle of wheel. This is an essential parameter in the simulation of ASM vehicle dynamics model to perform handling maneuvers in driving simulator. Steering wheel angle

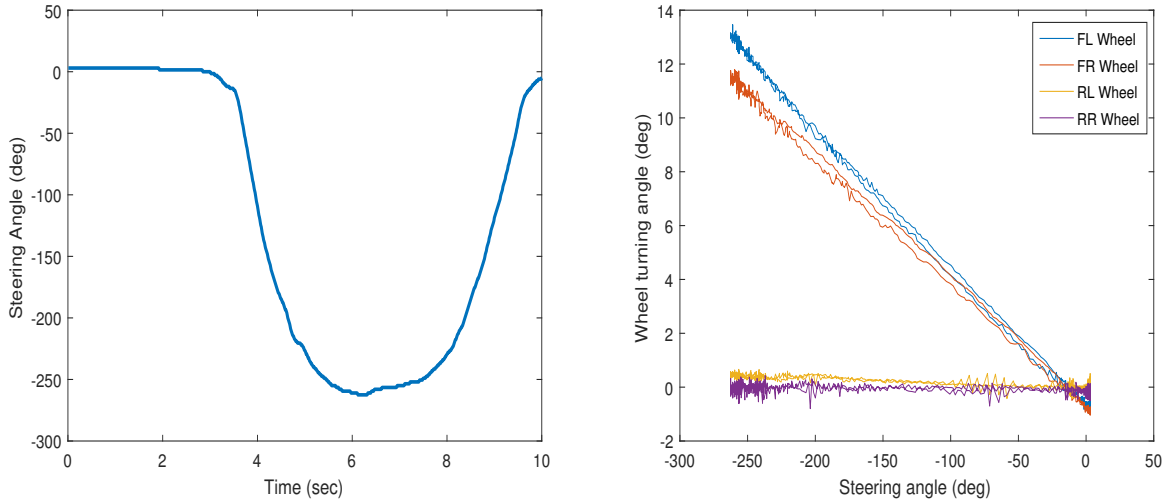

(a) (b)

Figure 5.7: Step steer test: (a) Steering angle vs time, (b) Wheel turning angle vs steering angle

is obtained from the CAN bus data and the wheel turning angle is obtained from WPS sensors that measure the orientation of wheel with respect to a reference frame on the body of the vehicle. Fig. 5.7 illustrates how the turning angle of each wheel changes with the change in steering wheel angle. It is evident from Fig. 5.7 that, both the rear wheels exhibit zero turning angle as the steering mechanism in Prius 2015 is connected only to the front wheels. It is also observed that for steering angles below 100°, both the front left and right wheels turned through the same amount. However, for higher steering angles, inner wheel turned through a higher angle than the outer wheel, which can be attributed to the Ackerman steering effect. As the focus of this research is in driving situations where the steering wheel angle generally doesn't exceed 100°, a constant steering ratio is chosen to determine the amount through which both left and right wheels turn.

5.5 Wheel inertia estimation

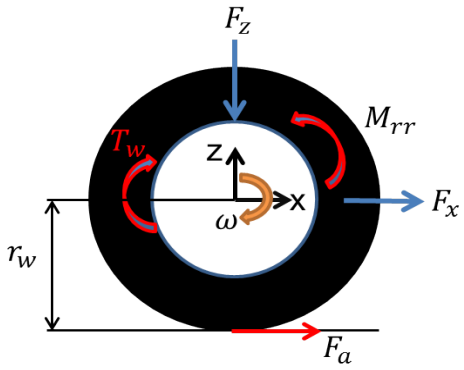

Figure 5.8: Forces and moments acting on the tire during longitudinal motion

Equation of motion representing the dynamics of front wheel rotation of Prius is given as:

$$\begin{aligned} J_w\dot{\omega} &= T_w - F_a r_{eff} - M_{rr} \\ M_{rr} &= f_{rr} F_z \end{aligned} \tag{5.12}$$

Also the longitudinal equation of motion of the wheel is given as:

$$m_w \dot{v}_x = F_x + F_a \tag{5.13}$$

where, J_w is the polar moment of inertia of tire-wheel assembly about the wheel rotation axis, T_w is the torque applied at wheel-hub, M_{rr} is the rolling resistance moment, F_a is the traction force, v_x is the longitudinal acceleration of the tire, r_w is the dynamic tire radius and m_w is the mass of the tire-wheel assembly. From equations (5.12) and (5.13), we obtain:

$$\omega = \int_{t1}^{t2} \frac{T_w - r_{eff}(F_x + m_w \dot{v}_x + f_{rr} F_z)}{J_w} dt \tag{5.14}$$

Equation (5.14) is solved to identify the wheel inertia utilizing the data recorded from VMS for T_w, ω, F_x,F_z, $\dot{v}$, and r_w. Non-linear least squares minimization is performed with F_x,

r_w, T_w, F_z, and m_w as inputs and ω as system output resulting in a J_w of 1.65 kgm^2. Fig. 5.9 shows the fit of estimated data against experimentally measured data.

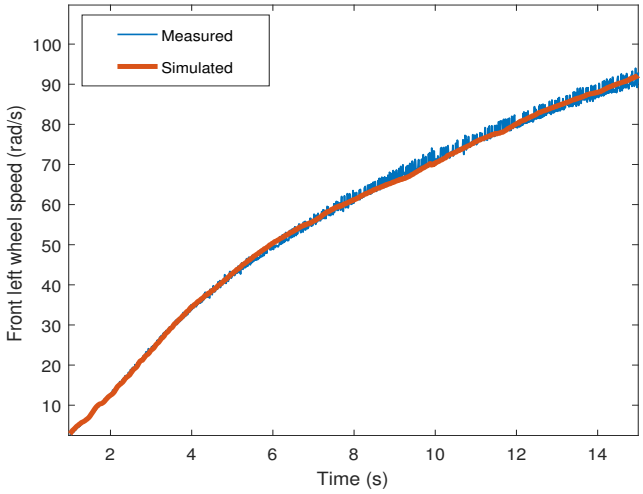

Figure 5.9: Angular wheel speed vs time

During the on-road testing, tires are equipped with sensors and rims of VMS that could contribute to the wheel rotary inertia. Also, processing signals from multiple sensors to obtain a single parameter (J_w) is not an ideal approach, as each signal could induce some sort of inaccuracy into the estimated parameter. Therefore, other approaches for estimating tire inertia have been investigated which include:

Simple pendulum testing: In simple pendulum test, Prius tire was suspended from a pivot point by a rope passing through the tire center as shown in Fig. 5.10a. The tire was given small initial angular displacement about the pivot point and time period of oscillations was recorded to calculate the natural frequency. A shift in the axis of rotation from pivot point to center of gravity of tire is accounted for in the final calculation of wheel inertia using parallel axis theorem. Wheel inertia is obtained as 1.25 kgm^2 by taking the average of multiple readings shown in Fig. 5.10b. It is observed that the finer readings of time period and shorter length of rope produced lesser deviation in the inertia estimates.

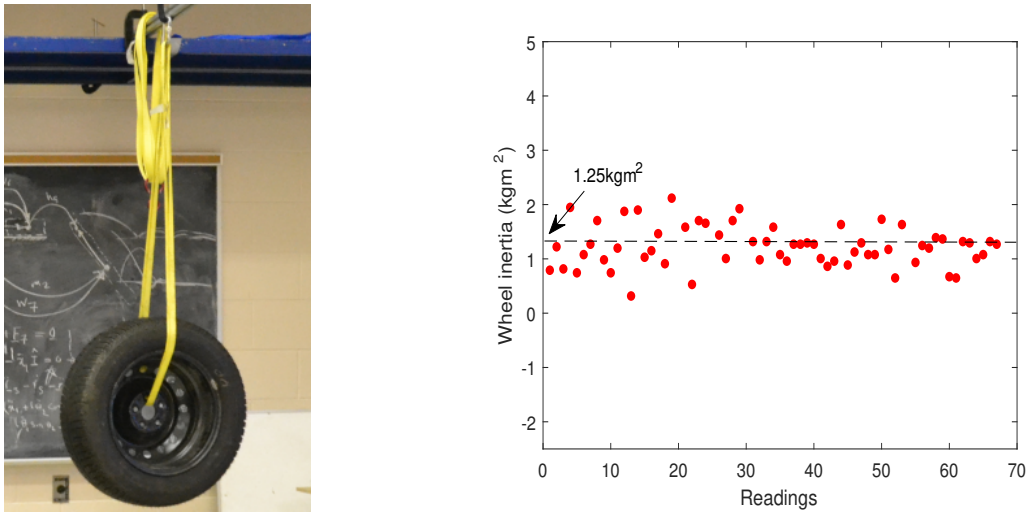

(a) (b)

Figure 5.10: Simple pendulum test: (a) Prius tire suspended by a rope and (b) Wheel inertia values from multiple readings

Vehicle jack up test: A comparatively simpler method of measuring wheel inertia to the ones mentioned above is by jacking up the front end of Prius equipped with WFS sensors as shown in Fig. 5.11a. After lifting the front end, brake pedal was pressed and released. Releasing the brake pedal caused the front wheels to rotate under the action of a small amount of torque. This procedure was carried out multiple times to make sure that the readings were consistent.

Torque and rotational speed of wheel are recorded from the measurements of WFS sensors and rotary encoders attached to that wheel. The inertia of wheel is estimated using equation (5.15) by taking the average of measurements shown in Fig. 5.11b. The sudden jumps in Fig. 5.11b at 0.6s and 1.8s represent the braking events.

$$J_w = \frac{T_w}{\dot{\omega}} \tag{5.15}$$

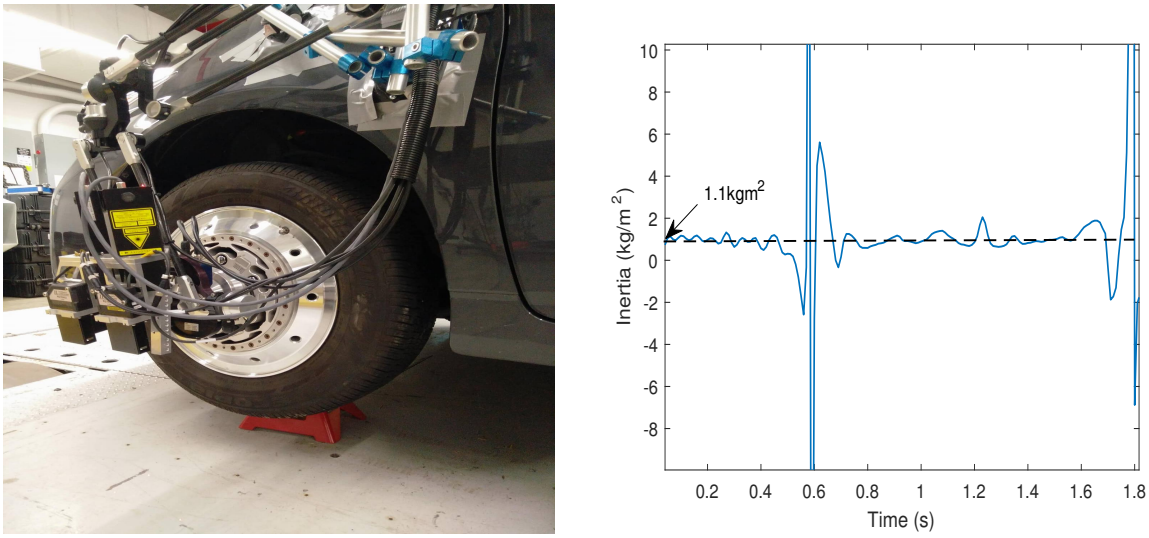

(a) (b)

Figure 5.11: Vehicle jack up test: (a) Lifted front end of Prius, (b) Wheel inertia vs time

5.6 Tire model parameter estimation

Tires are designed to be elastic in nature to reduce the vibrations from the road irregularities. This property of the tire causes it to deform while moving on a surface, which in the end results in the generation of forces and moments at the tire-surface contact patch. The predominant forces of interest for the tire development in this research include longitudinal and lateral forces, F_x and F_y. These forces are modelled in terms of the normal load (F_z) acting on tire and the slip (s) generated due to relative motion between tire and the surface on which it moves. Longitudinal slip (s_x) occurs when circumferential velocity of wheel ($r_w\omega$) is different from wheel travel velocity (v_x), whereas lateral slip(s_y) occurs when the contact patch slides horizontally and results in the angular difference between tire-plane of rotation and direction of motion.

According to the definition of JSAE670 [67], longitudinal and lateral slips are represented as:

$$s_x = \frac{r_w\omega - v_x}{v_x}, \quad s_y = \tan^{-1}\left(\frac{v_y}{v_x}\right) \tag{5.16}$$

$$F_x = C_x s_x, \quad F_y = C_y s_y \tag{5.17}$$

where, v_y, C_x and C_y represent the tire lateral velocity, longitudinal stiffness, and lateral stiffness. For small values of slip, tires exhibit linear behavior, in which case forces (F_x and F_y) are proportional to the amount of slip (s_x and s_y) at a given normal load as shown in equation (5.17). But, harsh acceleration, braking and handling maneuvers lead to higher slip values and introduce non-linear behaviour in tires. Pacejka's tire model relates the forces and moments at the contact patch to the normal load and slip using Pacejka's magic formula. It is a semi-empirical tire model whose first version introduced by Bakker et al. in 1986, models longitudinal force in terms of longitudinal slip (s_x) and lateral force in terms of slip angle (s_y) as shown in equation (5.19). This initial model didn't consider the effects from combined slip, inclination angle, and overturning moment. The version developed in 2002 is advanced and captures tire transient behavior realistically under extreme conditions of operation such as roll-over and racing events.

$$Y(s) = F_z(y(x) + S_v) \tag{5.18}$$

$$y(x) = D\sin\left[C\tan^{-1}Bx - E(Bx - \tan^{-1}Bx)\right] \tag{5.19}$$

$$x = s - S_h \tag{5.20}$$

where, $Y(s)$ is the quantity to be determined (F_x, F_y) and s is the independent variable (s_x, s_y). The four fitting coefficients B, C, D, E in equation (5.19) represent the stiffness, shape, peak, and curvature factors. The coefficients S_h and S_v represent the horizontal and vertical shifts in the curve $Y(s)$. The PAC 2002 model used in this research work requires 117 fitting coefficients to model a signal tire and identifying all these coefficients is a challenging task. However, 2002 model relies on the above mentioned coefficients to determine majority of the tire behaviour. Thus, these parameters are chosen to be identified from the experimental data.

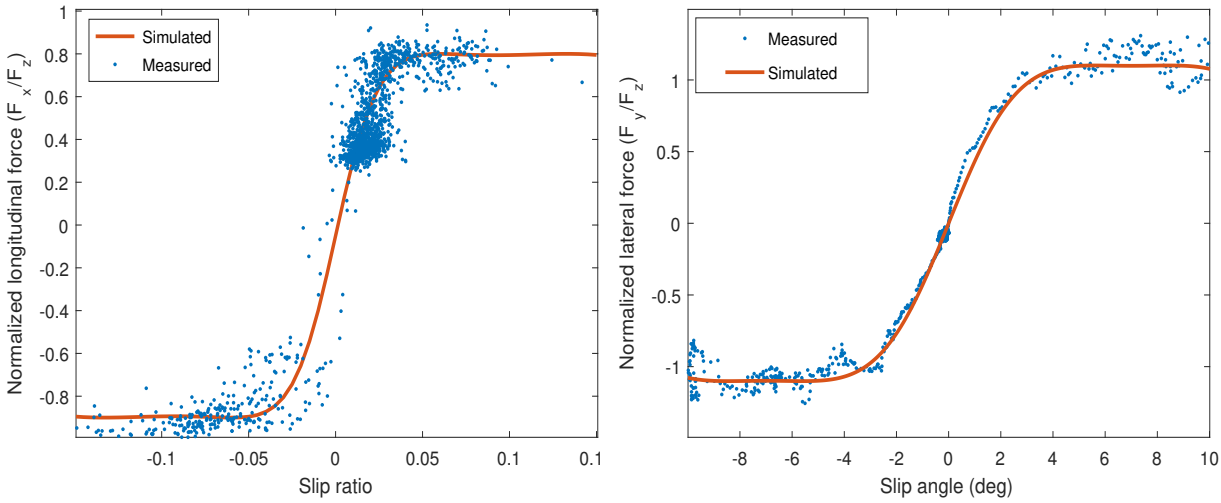

(a) (b)

Figure 5.12: Pacejka curve fits: (a) Normalized longitudinal force vs longitudinal slip and (b) Normalized lateral force vs lateral slip

The data from hard acceleration/braking and step steer maneuvers, which generate high longitudinal and lateral slip is used for the purpose of parameter identification. The tire forces (F_x, F_y) are measured by WFS sensors, while the longitudinal and lateral slip are derived using the measurements from LGS and LDV sensors. Parameters B, C, D, E, S_h and S_v are estimated by curve fitting the simulated values from equation (5.19) with the experimental data of normalized forces and moments as shown in Fig. 5.12. All the Pacejka tire parameters used to create Fig. 5.12a, 5.12b are listed in Table A.1. Longitudinal and lateral stiffness (C_x and C_y) of the tire are calculated by multiplying the slopes of normalized F_x and F_y curves (see Fig. 5.12a, 5.12b) with normal load at zero slip. The values of C_x and C_y are obtained as 169700N and 120000N respectively.

5.7 Half shaft stiffness and damping

Figure 5.13: Front left and right half shafts of Prius

Front left and right solid half shafts of the Prius PHEV 2015 with torsional dampers are shown in Fig 5.13. It can be seen that the shafts are of unequal length, which is often observed in vehicles with front-engine, front wheel drive layout. Structural steel is the commonly used material to manufacture a half shaft. Stiffness of these shafts is derived from their physical and material properties. Torsional stiffness (torque required per unit twist) of the shaft is expressed as:

$$K_{hs} = \frac{GJ_{hs}}{L_{hs}} \tag{5.21}$$

where, G is the modulus of rigidity, J_{hs} is the polar moment of inertia and L_{hs} is the length of shaft. Due to uneven diameter throughout the length, front left half shaft is modelled as a stepped shaft for finding its stiffness. Equivalent stiffness is calculated from the measurements of dimensions across different sections of each shaft. The torsional stiffness of right and left half shafts were obtained as 16576 and 29 292 Nm/rad respectively.

5.8 Driveline inertia estimation

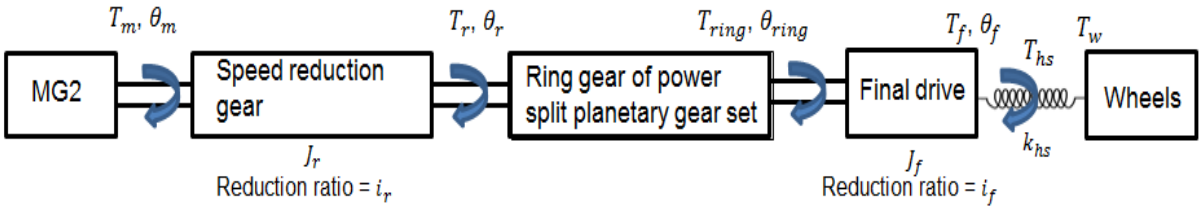

Figure 5.14: Schematic of torque transfer from motor (MG2) to wheels

The net inertia of rotating parts in the driveline affecting the transmitted torque, termed as driveline inertia, is estimated from the differential equations governing the rotational motion of these components. Due to the unavailability of experimental engine torque data, inertia of parts that are driven by motor (MG2) are only considered during the estimation process. Fig. 5.14 depicts the torque transfer from motor to wheels of the test vehicle through different subsystems considered in this work. The output torque from motor (T_m) is transmitted to ring gear through a speed reduction planetary gear set, with a gear ratio of i_r. Then, the ring gear transmits the torque via final drive, with a gear ratio of i_f, to the wheels. Frictional losses in the driveline components and torsional deformation of the half-shaft are neglected. From the Newton's second law for rotation, the equation of motion of these components is expressed as:

$$\begin{gathered} J_r\ddot{\theta}_r = T_m i_r - T_r \\ J_{ring}\ddot{\theta}_{ring} = T_r - T_{ring} \\ J_f\ddot{\theta}_f = T_{ring} i_f - T_f \\ T_f = 2T_{hs} = 2T_w \\ \theta_r = \theta_{ring}, \quad \theta_f = \frac{\theta_{ring}}{i_f}, \quad \text{and} \quad \theta_r = \frac{\theta_m}{i_r} \end{gathered} \tag{5.22}$$

Combining all the equations in 5.22, we obtain,

$$(J_r + J_{ring} + \frac{J_f}{i_f^2})\ddot{\theta}_m = T_m i_r^2 - \frac{2T_w i_r}{i_f} \tag{5.23}$$

where, $J_{f,r,ring}$, $T_{f,r,fing}$, $\theta_{f,r,ring}$ represent the inertia, output torques and angular rotations of the speed reduction gear, ring gear and final drive respectively. T_{hs} represents the half-shaft torque, T_w is the torque applied at the wheels and J_d $(J_r + J_{ring} + \frac{J_f}{i_f^2})$ is the driveline inertia which is to be determined.

Experimental data collected includes the motor torque and angular speed from vehicle CAN and the wheel torque from WFS sensors (VMS). Equation (5.23) is integrated and optimized simultaneously to minimize the objective function, which is the integral squared difference between the experimental and simulated motor speeds. Driveline inertia, J_d is estimated as $0.07\,\mathrm{kgm}^2$ and the correlation between experimental and simulated wheel speeds is shown in Fig. 5.16a.

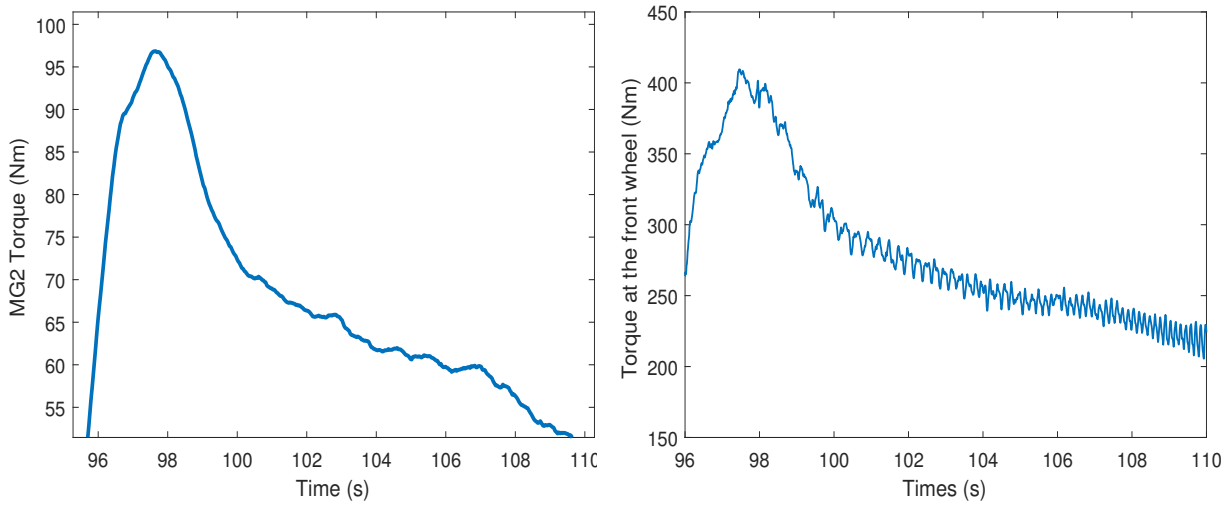

(a) (b)

Figure 5.15: Experimental data: (a) Motor (MG2) torque output from CAN signals and (b) Torque at the wheel hub from WFS sensors

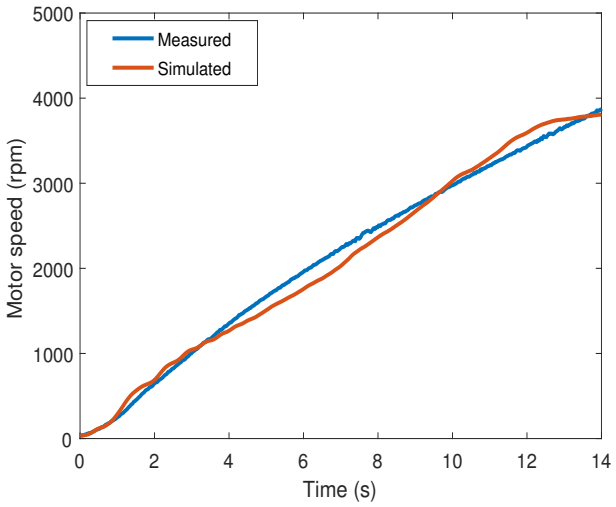

(a)

Figure 5.16: Comparison of simulated and experimental angular speeds of motor

5.9 Brake parameters

As mentioned in Chapter 3, a linear model was chosen for the mechanical braking system of the Prius. This brake model scales the brake pedal position linearly to determine the brake torque acting at the front and rear wheels. The corresponding scale factors are obtained by utilizing the data from a hard acceleration and braking maneuver. There are two main reasons for choosing this maneuver. The first is that, as the regenerative braking mode in Prius turns off automatically at high deceleration, the brake torque applied on the wheels is solely from mechanical braking. The other reason is that, this maneuver provides information about the maximum torques that can be applied on the front and rear wheels as shown in Fig. 5.17. Utilizing this data, simulation of full vehicle model is carried out to adjust the scaling factors associated with front and rear brakes. Additionally, this maneuver also provides sufficient information for hand tuning the parameters (maximum and minimum slip) of anti-lock braking system. The oscillations in the braking torque illustrated in Fig. 5.17 at maximum pedal depression are from the on-off action of ABS.

All the parameters associated with the brake model are listed in Table A.2.

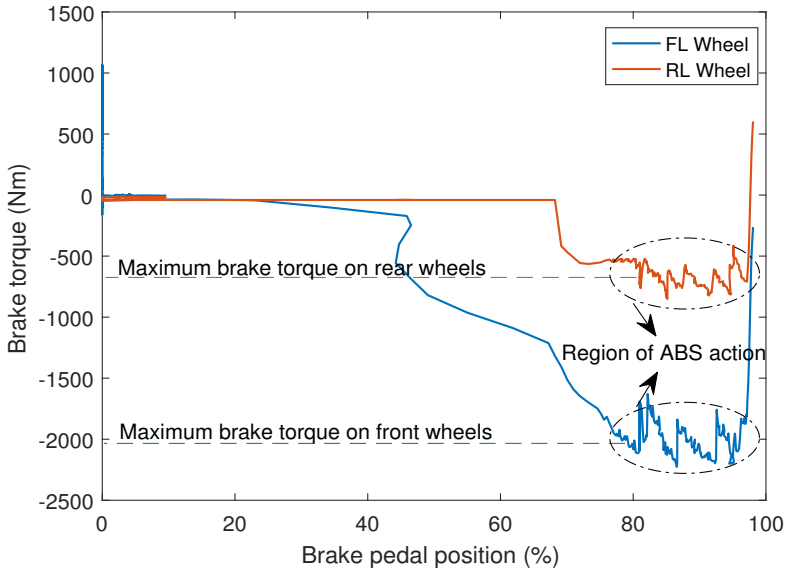

Figure 5.17: Plot of experimental brake torque vs brake pedal position data for front and rear wheels

5.10 Summary

This chapter presented different methods for obtaining the vehicle model parameters. Most of the parameters were obtained by minimizing the objective function formulated as the integral squared difference between the simulated and experimental values. Trust region reflective algorithm, a local optimization method, was used to find the arguments of the objective function. Homotopy, a global optimization method, was also investigated to confirm the convergence to global minimum. The vehicle parameters estimated in this chapter include CG location, frontal area, rolling resistance coefficient, suspension stiffness and damping, wheel inertia, tire model parameters, half shaft stiffness, steering ratio and brake parameters. The estimated suspension parameters showed a deviation of $\pm$ 10% from the results of 4-Post testing.

Chapter 6

Model validation

Once we have the fully developed vehicle dynamics model along with the important parameters obtained through parameter identification, the next step is to analyze the dynamic response of this model when supplied with these parameters. This chapter validates and discusses the simulation results of full vehicle models to determine if the desired characteristics are fulfilled. It should be noted that, any discrepancies between the simulation and experimental data could be a result of a combination of uncertainties in parameters or the simplifications/assumptions made during the model formulation.

In this chapter, simulations are executed for the following maneuvers: hard acceleration and braking, moderate acceleration and braking, steady state cornering, and double lane change. The results of MapleSim and ASM vehicle dynamics models are compared against the experimental data collected from the track testing of Prius in straight line maneuvers. The ASM model is further validated using the experimental data from handling maneuvers to ensure its successful implementation in the driving simulator. In these simulations, the models are supplied with three inputs: 1) torque from the power train, 2) position of the brake pedal, and 3) steering wheel angle (ASM only). The engine torque signal is unavailable in the collected experimental data. Consequently, for the tests conducted in hybrid mode, the torque input to the model is derived from the WFS sensor measurements.

6.1 Longitudinal vehicle dynamics

Longitudinal dynamics is evaluated by analyzing simulated vehicle speed, acceleration, and slip generated at the tire contact patch. The experimental data of these signals is used to validate the response of MapleSim and ASM vehicle dynamics for the maneuvers discussed below.

6.1.1 Straight line hard acceleration and braking

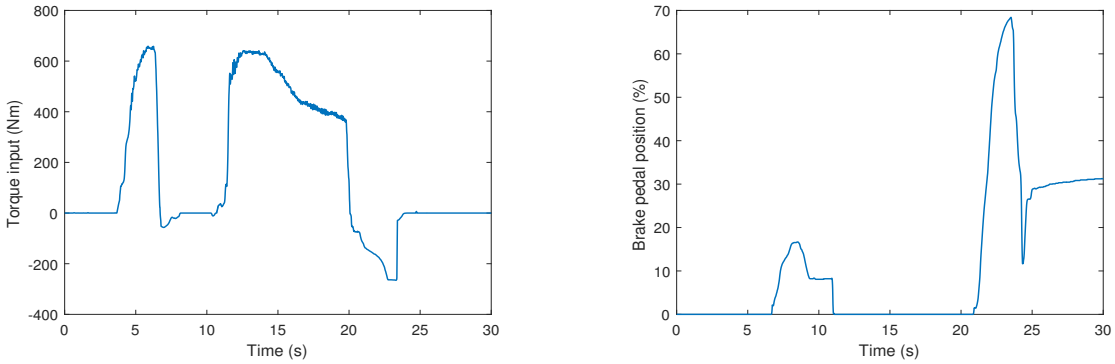

(a) (b)

Figure 6.1: Hard acceleration and braking test: (a) Input torque from the powertrain and (b) Brake pedal depression (%) vs time

Straight line hard acceleration and braking maneuver was performed in hybrid mode. In this maneuver, the engine assists the motor to provide the torque demanded for rapid acceleration. Also, as the brake pedal is depressed to the maximum extent, friction braking plays a significant role in bringing the vehicle to rest. To the study the longitudinal dynamics in these hard acceleration and braking events, the models are supplied with two inputs. These include the torque supplied by the power train and the brake pedal position (% of maximum range) as shown in Fig. 6.1. The input torque profile is obtained by combining the data from WFS sensors and CAN signals. The negative region in the torque input profile represents the regenerative brake torque applied by the motor/generator (MG2).

Also, the steering input to the ASM model is zero as it is a straight line driving maneuver. Both the models are given a very low initial speed of 0.15 m/s at the beginning of the simulation to avoid numerical instability.

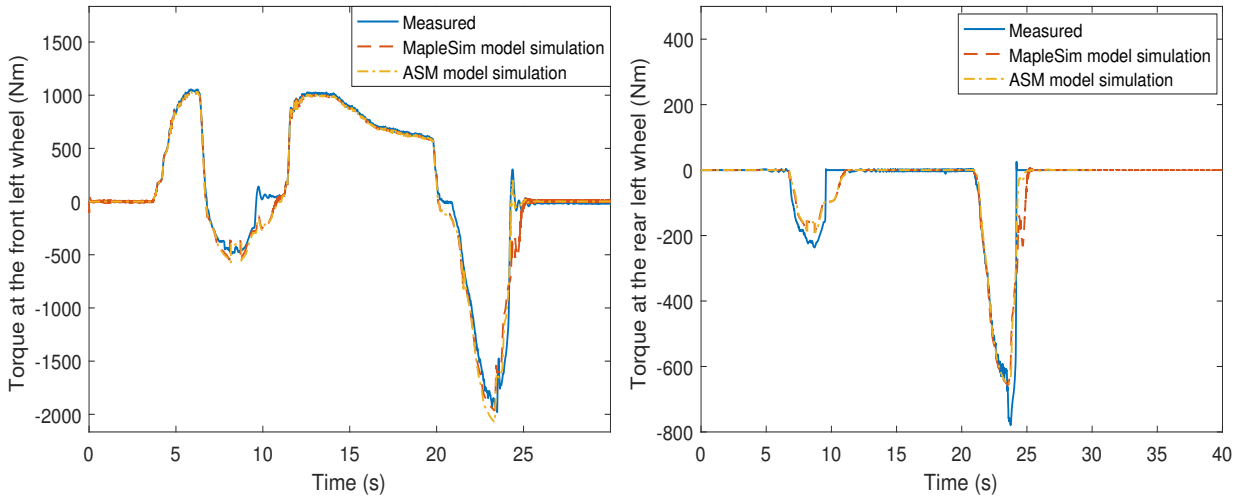

(a) (b)

Figure 6.2: Hard acceleration and braking test: (a) Torque at the front wheels and (b) Torque at the rear wheels

Plots shown in Fig. 6.3 and 6.2 indicate that both the models are sufficiently accurate to replicate the behavior of Prius in a hard acceleration and braking maneuver. However, the linear brake system in both vehicle models was not capable of reproducing the desired torque during the first braking event. This insufficiency in the brake torque resulted in a delay of 1 sec to bring the vehicle to rest. The delay can be clearly observed in Fig. 6.3a, where the simulated speeds are compared against the experimental data.

Fig. 6.4 shows the longitudinal slip generated in this maneuver, which is quite high. Such high ratio implies that the front tires in both models are exhibiting non-linear behavior. Fig. 6.4 also depicts MapleSim model's high frequency oscillations in the longitudinal slip only at zero speed (t=11 s). Surprisingly, such oscillations in the ASM model occur at all speeds below 3 m/s. These oscillations at zero speed are expected because of the

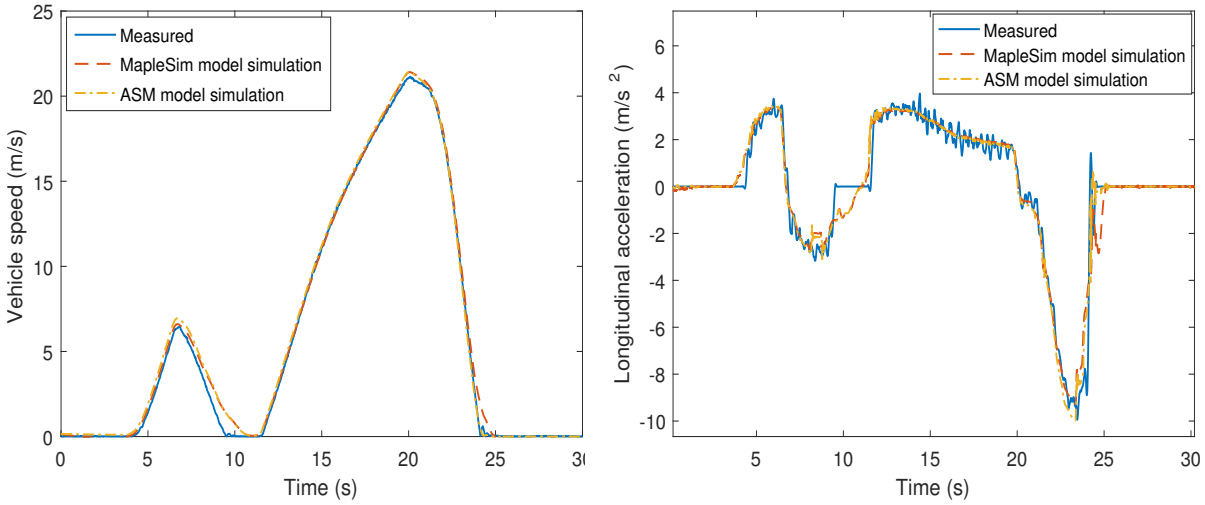

(a) (b)

Figure 6.3: Hard acceleration and braking test: (a) Vehicle speed and (b) Vehicle acceleration

vehicle speed term in the denominator of the slip equation (5.16). But, the oscillations in ASM model at low velocities and the discrepancies in the slip between two models could be due to various factors. Some of these include using default values in maps (wheel z displacement-spring displacement and wheel z displacement-damper displacement) for suspension kinematics, numerical formulation of the ASM's system (MapleSim performs symbolic computation and uses polynomial approximations to avoid sudden jumps in signals), and discrete integration of the ASM's system equations (MapleSim does continuous integration). Nevertheless, the tire dynamics incorporated in ASM model avoids the influence of these oscillations on the estimated tire force by introducing additional damping at low vehicle speeds. Eventually, these high frequency oscillations are not apparent in the simulated vehicle speed shown in Fig 6.3a.

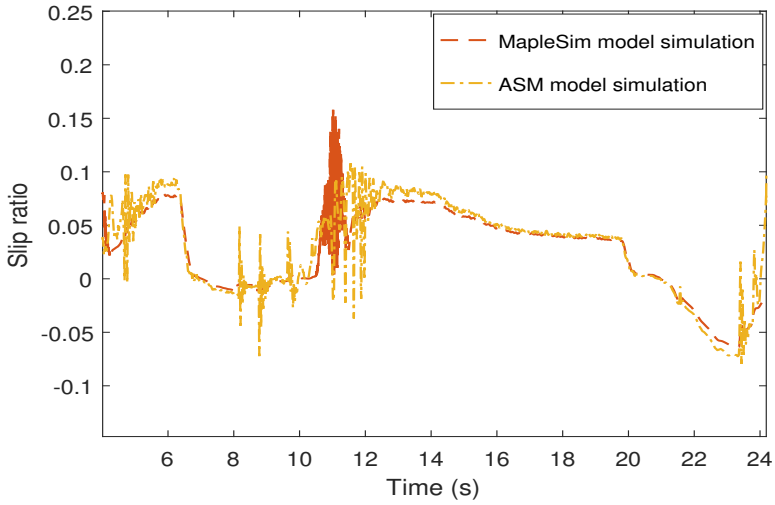

Figure 6.4: Hard acceleration and braking test: Simulated longitudinal slip vs time

6.1.2 Straight line moderate acceleration and braking

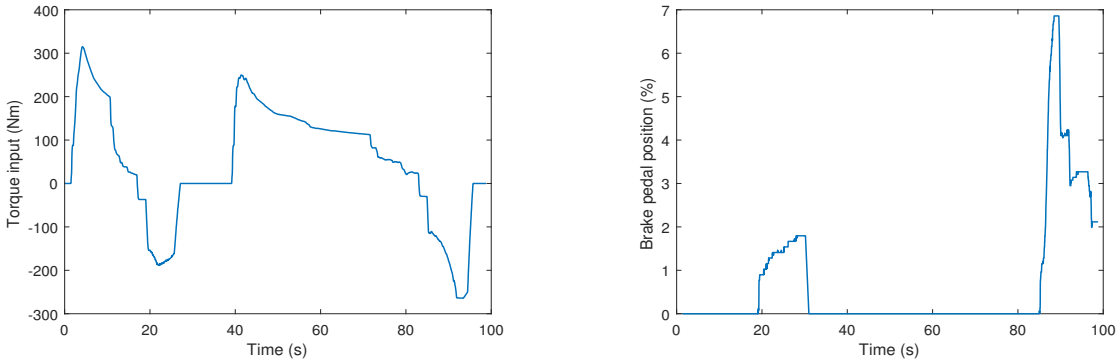

(a) (b)

Figure 6.5: Moderate acceleration and braking test: (a) Input torque from the powertrain and (b) Brake pedal depression (%) vs time

Moderate acceleration and braking maneuver is performed in EV mode. It consists of two acceleration and braking events with vehicle speeds reaching up to 40 and 80km/hr. The

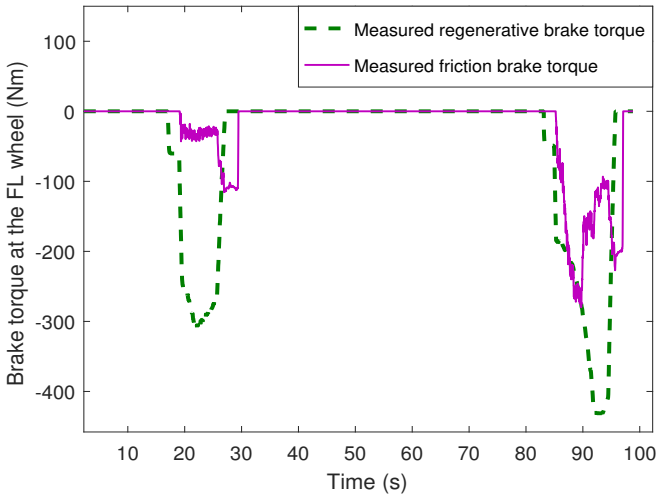

Figure 6.6: Moderate acceleration and braking test: comparison of the experimental regenerative brake torque and friction brake torque acting at the front left wheel

inputs to the models, shown in Fig. 6.5, are the torque supplied by the powertrain and the position of the brake pedal, obtained from CAN bus data. Note that the brake pedal depression, as illustrated in Fig. 6.5b, is very low. Comparison of experimental regenerative brake torque against the friction brake torque in Fig. 6.6 shows that most of the brake torque in this maneuver is from the regeneration. Similar to the previous maneuver, both models are given an initial velocity of 0.15 m/s at the beginning of simulation. Fig. 6.7d clearly shows that maximum acceleration produced in this maneuver is nearly half of what is observed in the previous maneuver. Hence, the tires are supposed to exhibit linear behaviour throughout the maneuver.

It can be seen from Fig. 6.7a that both models are adequate enough to reproduce the torque acting at the front wheels during acceleration. However, it is observed that experimental data of front and rear brake torques during the brake pedal release (at 30 and 96 s) do not correlate with the torques produced from the linear brake model. This discrepancy resulted in slightly longer stopping distances in the model simulation. A non-linear map or physical model for brakes could improve these results.

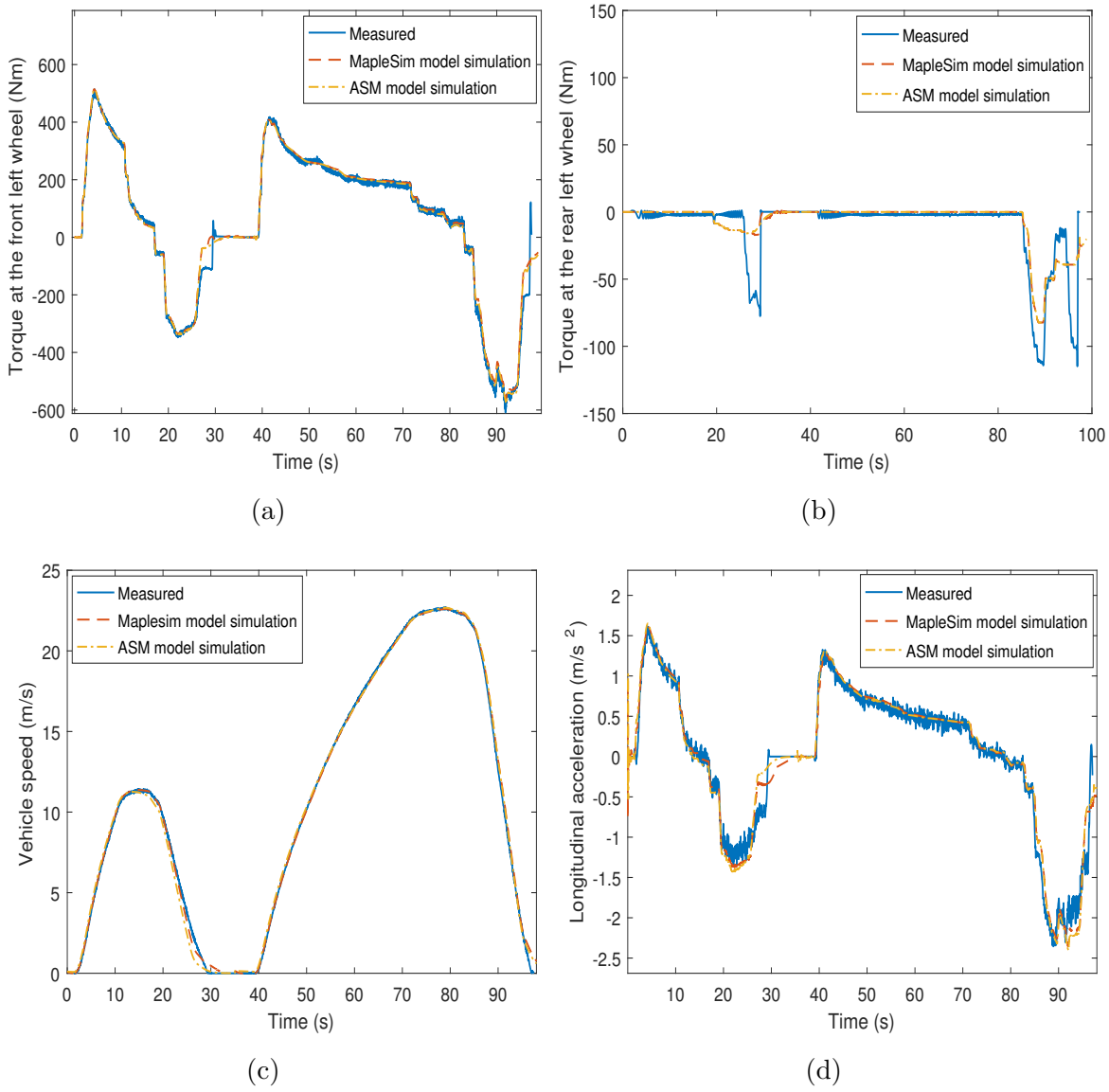

Figure 6.7: Moderate acceleration and braking test: (a) Torque at front wheels, (b) Torque at the rear wheels, (c) Vehicle speed, and (d) Vehicle acceleration

6.2 Vehicle handling dynamics

Handling dynamics of ASM model is evaluated in the form of simulated yaw rate, roll rate, pitch rate and lateral acceleration acting at the CG of the ASM vehicle model. These results are validated using the experimental data for the maneuvers discussed below.

6.2.1 Steady state cornering test

The steady state cornering test (ISO 4138) is commonly used to evaluate the yaw response and lateral acceleration of the vehicle in steady state conditions. At a particular speed, a smaller circular turn radius produces higher yaw rate and lateral acceleration. In the steady state cornering test performed for this research, vehicle is driven on circle with a constant radius of 15 m. While following this course, the vehicle speed is slowly increased and maintained constant at the maximum attainable value. For the simulation of this maneuver, the ASM model was given two inputs. The first is the torque input obtained directly from the signals recorded by WFS sensors. The other input is the steering wheel angle, as shown in Fig. 6.8, recorded by the vehicle CAN. As the steering angle is almost constant throughout this maneuver, roll rate achieved by the vehicle is quite low.

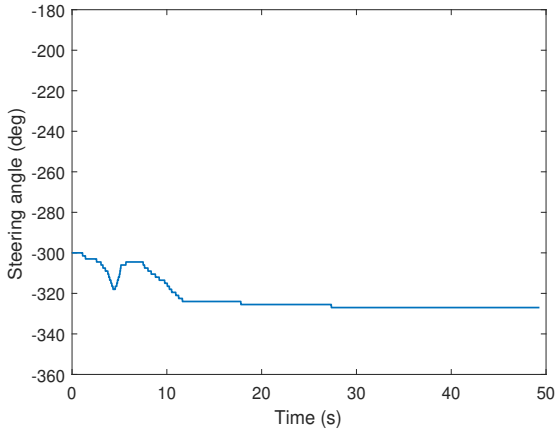

Figure 6.8: Steady state cornering test: Steering wheel angle vs time

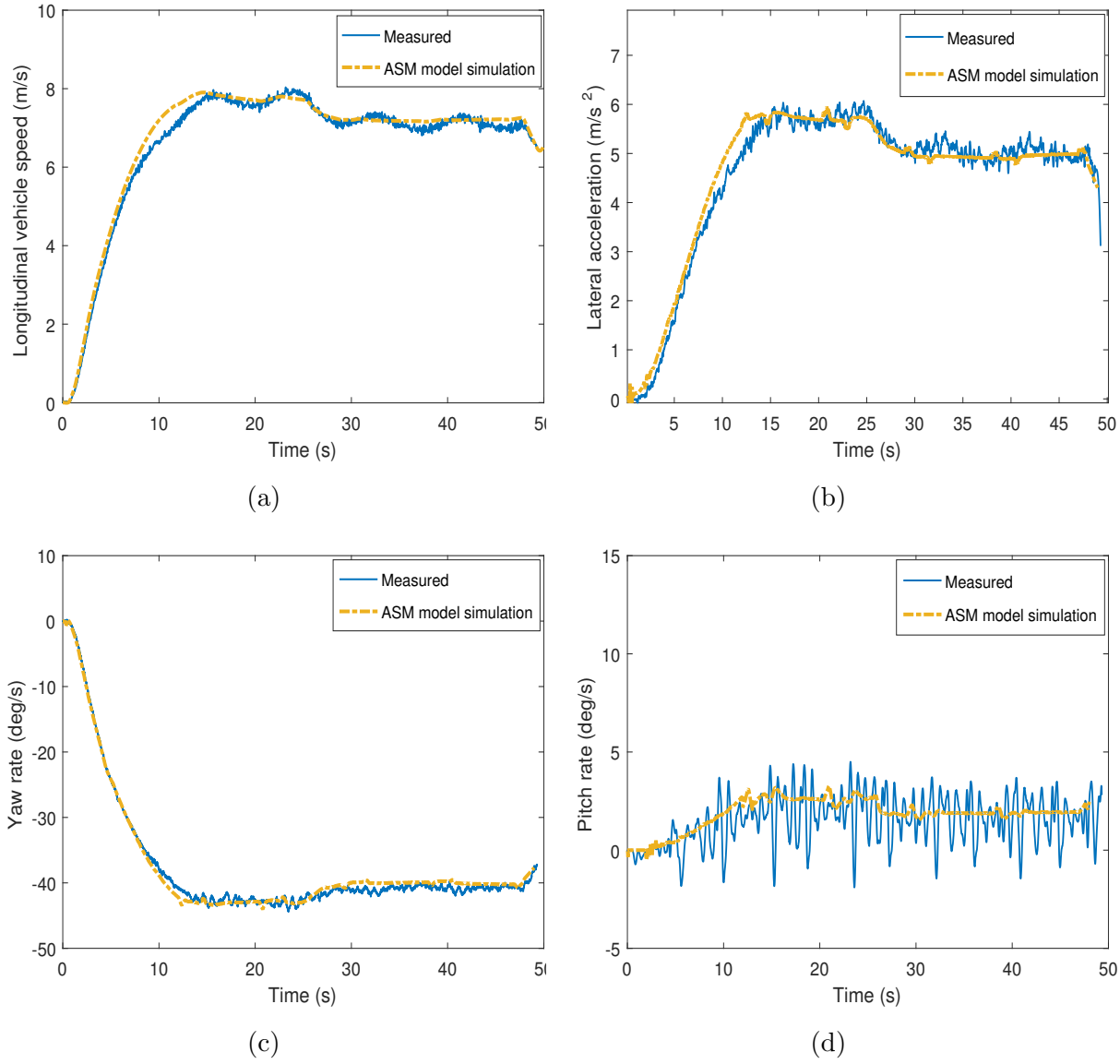

Figure 6.9: Steady state cornering test: (a) Longitudinal vehicle speed, (b) Lateral acceleration, (C) Yaw rate, and (d) Pitch rate

Fig. 6.9 shows the comparison of longitudinal speed, yaw rate, pitch rate and lateral acceleration simulated by the model against the experimental data obtained for this ma-

neuver. Plots of yaw rate and lateral acceleration match very well with the experimental data even at the high speeds. This indicates that the steering ratio and the tire model parameters that determine the forces at the tire contact patch are accurate enough to reproduce the handling maneuvers in steady state situations.

6.2.2 Double lane change maneuver

The double lane change maneuver (ISO 3888-1) is commonly used to examine the transient response of the vehicle. In the double lane change maneuver performed for this research, vehicle is initially driven in a straight line to a maximum speed of 53km/hr. It is then steered to follow a trajectory prescribed by the cones, while maintaining the speed at the maximum achieved value. Fig. 6.10 shows the steering input given to the ASM model for simulating this maneuver. In contrast to the previous maneuver, the steering angle here changes quite rapidly from -60° to +60° producing a significant roll rate.

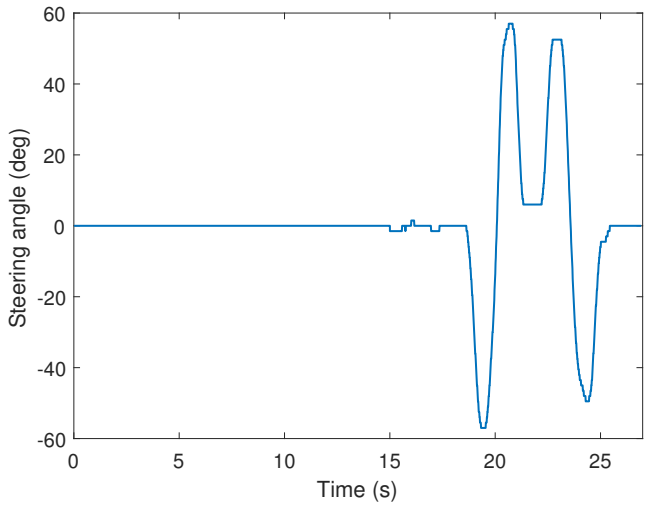

Figure 6.10: Double lane-change maneuver: Steering wheel angle vs time

Fig. 6.11 shows the comparison of experimental data against the longitudinal speed, yaw rate, roll rate and lateral acceleration simulated by the model for this maneuver.

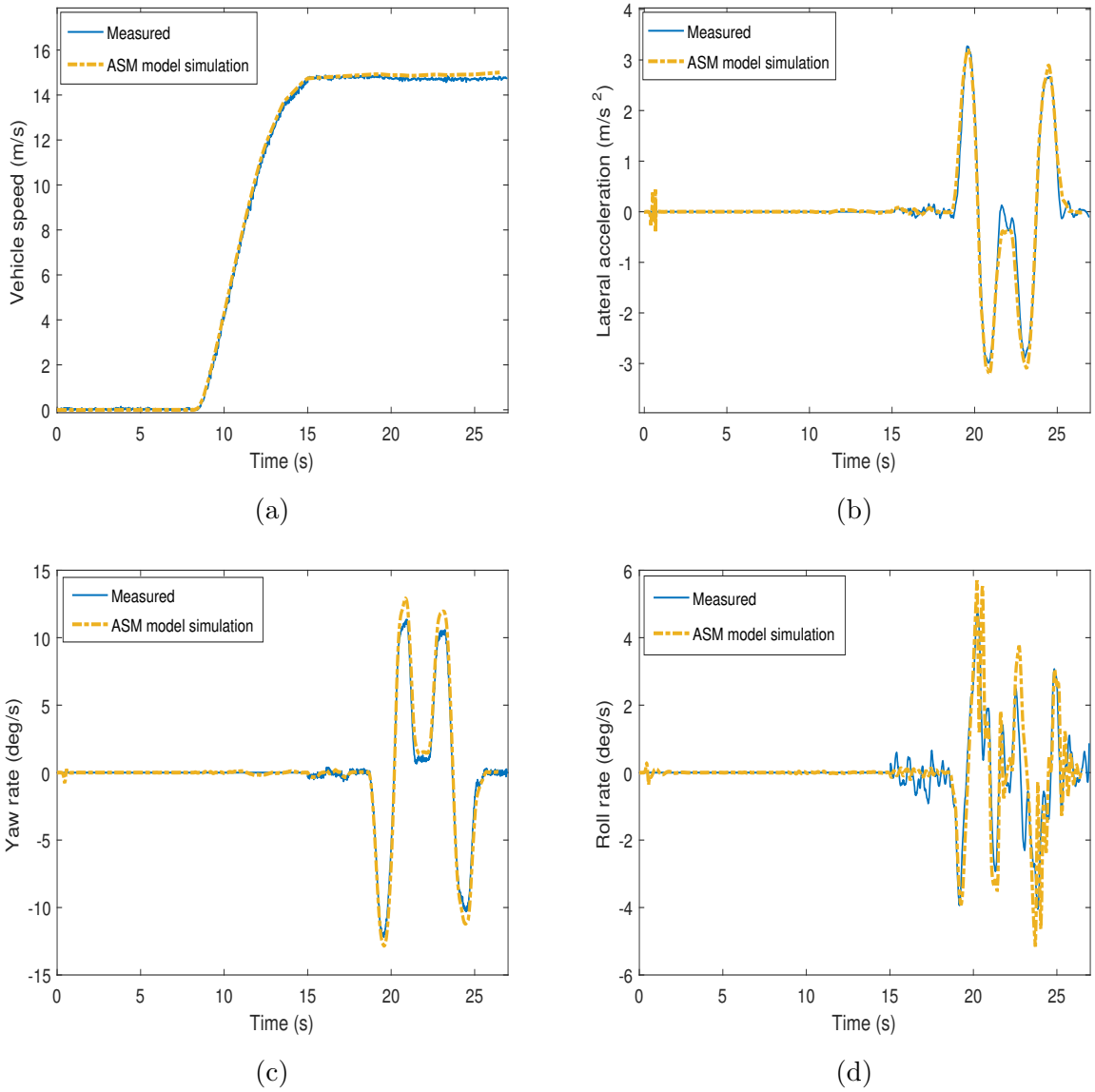

Figure 6.11: Double lane-change maneuver: (a) Longitudinal vehicle speed, (b) Lateral acceleration, (C) Yaw rate, and (d) Roll rate

Although the plots match well, simulation results showed slight deviation from the experimental data whenever there is change in the direction of the steering wheel rotation. The root-mean-square deviation (RMS) of the simulated yaw rate, roll rate, and lateral acceleration are obtained as 11.30%, 20.10%, and 10.89% respectively. This implies that the model is simply not able to reproduce the fast dynamics exhibited by the real vehicle during unexpected turns. There are a lot of factors influencing the behavior of the vehicle model in such rapid conditions. For example, the first order tire dynamics [68] incorporated in the vehicle dynamics model is inadequate to capture the transient conditions. However, these differences are small enough to be neglected for the intended purpose of this model, i.e. during normal driving conditions.

6.3 Summary

The chapter presented the simulation results of vehicle dynamics models for the straight line and handling maneuvers. Longitudinal response of the developed models was evaluated by simulating the moderate and hard acceleration/braking maneuvers. It was observed that insufficient brake torque generated from the linear brake model resulted in a slight delay in the vehicle stopping time. Also, the high frequency oscillations in simulated longitudinal slip and the possible causes were discussed. Additionally, to evaluate the handling response of the ASM model, the steady state cornering and double lane change maneuvers were simulated. The results of yaw rate, roll rate, pitch rate and lateral acceleration from the model simulation compared well with the data obtained in steady state conditions. However, simulated values of yaw rate and lateral acceleration were slightly higher in transient conditions. Despite of these minor discrepancies, the results of vehicle response in 6DOF are realistic and displayed a sufficiently good agreement with the experimental data.

Chapter 7

Conclusions

This thesis has presented the development of two validated vehicle dynamics models of Prius PHEV by employing different techniques to identify the model parameters. The first model, developed in MapleSim, is a longitudinal vehicle dynamics model, which will be used to evaluate the performance of various controllers that aim at minimizing the fuel consumption. This model was developed from scratch utilizing the components from multibody, tire, and hydraulics libraries in MapleSim. Minimal complexity, reduced degrees of freedom, and symbolic computing ensured the MapleSim model to be real-time implementable. The second model presented in this thesis is a modification to the detailed generic vehicle model in ASM vehicle dynamics software that supports the virtual vehicle simulation in the driving simulator. The brake and steering modules of the generic ASM model were altered to be based on scale factors and steering ratio, respectively. This model was also integrated with the anti-lock braking system exported from MapleSim as an S-function.

In contrast to the existing practices for parameter estimation that require standardized test facilities, extensive data processing, and filtering, this thesis presented an alternative to estimate the vehicle dynamics parameters. Here, the vehicle parameters were estimated using the on-road vehicle data collected from the VMS sensors, GPS, IMU and CAN bus signals. This manner of estimating parameters from on-road data takes into account all the factors encountered by a vehicle on the real road. In this thesis, every parameter

identification problem targeting a specific set of vehicle parameters was posed as a non-linear least squares problem. The objective function, formulated as an integral squared difference between simulated and experimental values was minimized using a local optimization method, called trust-region reflective. The methods to identify vehicle dynamics parameters associated with CG, suspension, tire, steering, brakes and half-shafts were explained comprehensively in Chapter 5. Moreover, a global optimization method known as homotopy, which is a hybrid of stochastic and deterministic methods of optimization, was investigated to identify suspension parameters. Comparison with the results of homotopy showed that the parameters estimated from the trust region reflective algorithm were successfully converging to a global minimum.

Prius was also tested on the 4-Post test rig, a standardized test rig for obtaining suspension characteristics. It was observed that the suspension parameters determined from the speed bump testing proposed in this thesis showed a deviation of $\pm 10\%$ from the values obtained through 4-Post testing. Some possible reasons behind such deviation are the change in the tire characteristics while rolling on the road or the linearity in the suspension elements assumed during model formulation.

Finally, in Chapter 6, the MapleSim and ASM models were supplied with the estimated parameters and validated using the experimental data from real road driving maneuvers. These included hard acceleration and braking, moderate acceleration and braking, steady state circular cornering and double lane change maneuvers. Some secondary parameters (see Table A.2), which haven't been identified in this work, were set to their default values for the functioning of the models. Comparison of experimental data with the simulation results suggested that a satisfactory match was obtained in the 6-DOF motions of the vehicle, which are probably the most important results, considering the scope of this research work.

7.1 Contributions

The main contribution of this thesis is in the development and parameter identification of the real-time implementable vehicle dynamic models of Toyota Prius PHEV. The models

are validated with the experimental data from real road driving conditions.

7.2 Future work

This research can be further improved and extended in the following directions:

ASM vehicle model: The slip estimation in the ASM tire model can be improved by including relaxation length effect [69], which could mitigate the high frequency oscillations observed in slip results.

MapleSim model: The MaplSim model can be made as a full fledged vehicle dynamics model, by including a steering system and adding non-linear characteristics to dampers in the suspension system.

Driving simulator implementation: So far, this research work dealt only with the vehicle dynamics of the ASM vehicle model. But, to implement this model on the driving simulator, it must have a powertrain model of Prius which accepts the throttle and brake pedal inputs from driver. This can be done by importing an Autonomie power train model of Prius into ASM's Simulink environment and combining it with the validated vehicle dynamics model developed in this thesis.

Parameter identification: Below are some suggestions for improving the parameter identification methods.

- In this work, the model used for CG identification considered the vehicle as a rigid body, neglecting the effect of suspension. This assumption can be avoided and the accuracy of CG height can be improved by using a half-car suspension model.
- Identifying the driveline inertia including the contribution from engine inertia, if the engine torque signal is available simultaneously with motor/generator torque signals.
- Developing a non-linear map of brake-torque vs brake-pedal position can improve the results of estimated brake torque.
- Identifying parameters, such as yaw inertia, roll inertia, Pacejka tire model's combined slip coefficients, which haven't been discussed in this work.

- Estimating the parameters of half car suspension model using the raw data obtained from 4-Post testing. Comparison of the parameters so obtained against the values from Multimatic's model could suggest inaccuracies associated with the modeling.

References

[1] M. Broy, I. H. Kruger, A. Pretschner, and C. Salzmann, "Engineering automotive software," *Proceedings of the IEEE*, vol. 95, no. 2, pp. 356–373, 2007.

[2] N. Instruments, "The Evolution of Real-Time Testing," http://www.ni.com/newsletter/51110/en/, retrieved: 2017.06.06.

[3] M. Vajedi, "Real-Time Optimal Control of a Plug-in Hybrid Electric Vehicle Using Trip Information," Ph.D. dissertation, University of Waterloo, Canada, 2016.

[4] M. Blundell and D. Harty, *The multibody systems approach to vehicle dynamics*. Elsevier, 2004.

[5] P. S. Rao, D. Roccaforte, R. Campbell, and H. Zhou, "Developing an adams® model of an automobile using test data," SAE Technical Paper, Tech. Rep., 2002.

[6] A. Hall and J. McPhee, "Automation of Adams/Car K&C correlation using MATLAB," SAE Technical Paper, Tech. Rep., 2014.

[7] CarSIM, "CarSIM Brochure," https://www.carsim.com/downloads/pdf/carsim_brochure.pdf, retrieved: 2017.06.06.

[8] N. Biggs, E. K. Lloyd, and R. J. Wilson, *Graph Theory, 1736-1936*. Oxford University Press, 1976.

[9] H. E. Koenig, Y. Tokad, and H. K. Kesavan, *Analysis of Discrete Physical Systems*. McGraw-Hill (New York), 1967.

[10] S. Seshu and M. B. Reed, *Linear graphs and electrical networks*. Addison-Wesley, 1961.

[11] G. C. Andrews and H. K. Kesavan, "The vector-network model: a new approach to vector dynamics," *Mechanism and Machine Theory*, vol. 10, no. 1, pp. 57–75, 1975.

[12] P. Shi and J. McPhee, "Dynamics of Flexible Multibody Systems Using Virtual Work and Linear Graph Theory," *Multibody System Dynamics*, vol. 4, no. 4, pp. 355–381, 2000.

[13] C. Schmitke, K. Morency, and J. McPhee, "Using graph theory and symbolic computing to generate efficient models for multi-body vehicle dynamics," *Proceedings of the Institution of Mechanical Engineers, Part K: Journal of Multi-body Dynamics*, vol. 222, no. 4, pp. 339–352, 2008.

[14] J. Banerjee, "Graph-theoretic Sensitivity Analysis of Dynamic Systems," Ph.D. dissertation, UWSpace, 2013.

[15] A. Hall, T. Uchida, F. Loh, C. Schmitke, and J. Mcphee, "Reduction of a vehicle multibody dynamic model using homotopy optimization," *Archive of Mechanical Engineering*, vol. 60, no. 1, pp. 23–35, 2013.

[16] A. Taghavipour, "Real-time optimal energy management system for plug-in hybrid electric vehicles," Ph.D. dissertation, University of Waterloo, Canada, 2014.

[17] K. M. Roberts, "FHWA highway driving simulator," *Public Roads*, vol. 44, no. HS-031 069, 1980.

[18] E. Blana, *A Survey of Driving Research Simulators Around the World*. Institute of Transport Studies, University of Leeds, 1996.

[19] A. R. W. Huang and C. Chen, "A low-cost driving simulator for full vehicle dynamics simulation," *IEEE Transactions on Vehicular Technology*, vol. 52, no. 1, pp. 162–172, 2003.

[20] G. Weinberg and B. Harsham, "Developing a low-cost driving simulator for the evaluation of in-vehicle technologies," in *Proceedings of the 1st International Conference on Automotive User Interfaces and Interactive Vehicular Applications*. ACM, 2009, pp. 51–54.

[21] R. W. Allen, S. J. Woon, G. D. Park, and J. K. Grant, "The development of a low cost driver licensing simulator," *Actes INRETS*, pp. 221–229, 2010.

[22] T. Shiiba and Y. Suda, "Development of driving simulator with full vehicle model of multibody dynamics," *JSAE review*, vol. 23, no. 2, pp. 223–230, 2002.

[23] J. Andreasson, N. Machida, M. Tsushima, J. Griffin, P. SundstrÃ *et al.*, "Deployment of high-fidelity vehicle models for accurate real-time simulation," in *The First Japanese Modelica Conferences, May 23-24, Tokyo, Japan*, no. 124. Linköping University Electronic Press, 2016, pp. 78–86.

[24] M. Dempsey, G. Fish, and A. Picarelli, "Using Modelica models for Driver-in-the-loop simulators," in *Proceedings of the 9th International MODELICA Conference; September 3-5; 2012; Munich; Germany*, no. 076. Linköping University Electronic Press, 2012, pp. 571–578.

[25] J. Gómez Fernández, "A Vehicle Dynamics Model for Driving Simulators," Master's thesis, Chalmers University of Technology, Sweden, 2012.

[26] E. Obialero, "A refined vehicle dynamic model for driving simulators," Ph.D. dissertation, Master Thesis in Automotive Engineering, Department of Applied Mechanics, Chalmers University of Technology, Goteborg, Sweden, 2013.

[27] M. K. Salaani, C. Schwarz, G. J. Heydinger, and P. A. Grygier, "Parameter determination and vehicle dynamics modeling for the national advanced driving simulator of the 2006 BMW 330i," SAE Technical Paper, Tech. Rep., 2007.

[28] M. K. Salaani and G. J. Heydinger, "Model validation of the 1997 Jeep Cherokee for the National Advanced Driving Simulator," SAE Technical Paper, Tech. Rep., 2000.

[29] M. K. Salaani and G. J. Heydinger, "Powertrain and brake modeling of the 1994 Ford Taurus for the National Advanced Driving Simulator," SAE Technical Paper, Tech. Rep., 1998.

[30] A. A. Prinz, "Neuronal Parameter Optimization," scholarpedia 2:1903., 2007.

[31] S. Saelid, *Process Identification Techniques*. Dordrecht: Springer Netherlands, 1995, pp. 81–97.

[32] H. Rahimi-Eichi and M. Chow, "Adaptive parameter identification and state-of-charge estimation of lithium-ion batteries," in *IECON 2012-38th Annual Conference on IEEE Industrial Electronics Society*. IEEE, 2012, pp. 4012–4017.

[33] J. Hahn, R. Rajamani, and L. Alexander, "Gps-based real-time identification of tire-road friction coefficient," *IEEE Transactions on Control Systems Technology*, vol. 10, no. 3, pp. 331–343, 2002.

[34] M. Rozyn and N. Zhang, "A method for estimation of vehicle inertial parameters," *Vehicle system dynamics*, vol. 48, no. 5, pp. 547–565, 2010.

[35] A. Vahidi, A. Stefanopoulou, and H. Peng, "Experiments for online estimation of heavy vehicles mass and time-varying road grade," in *ASME 2003 International Mechanical Engineering Congress and Exposition*. American Society of Mechanical Engineers, 2003, pp. 451–458.

[36] K. Erguler and M. P. H. Stumpf, "Practical limits for reverse engineering of dynamical systems: a statistical analysis of sensitivity and parameter inferability in systems biology models," *Molecular BioSystems*, vol. 7, no. 5, pp. 1593–1602, 2011.

[37] W. F. Milliken, D. L. Milliken *et al.*, *Race car vehicle dynamics*. Society of Automotive Engineers, Warrendale, 1995, vol. 400.

[38] C. B. Winkler, K. L. Campbell, and C. Mink, "Center of gravity height: a round-robin measurement program," Tech. Rep., 1991.

[39] N. Mango, "Measurement & Calculation of Vehicle Center of Gravity Using Portable Wheel Scales," SAE Technical Paper, Tech. Rep., 2004.

[40] R. S. Sharp, *The measurement of mass and inertial properties of vehicles and components.* Institution of Mechanical Engineers, London (England), 1997.

[41] W. R. Garrott, M. W. Monk, and J. P. Chrstos, "Vehicle inertial parameters-measured values and approximations," Tech. Rep., 1988.

[42] C. B. Winkler, "Measurement of inertial properties and suspension parameters of heavy highway vehicles," SAE Technical Paper, Tech. Rep., 1973.

[43] C. Doniselli, M. Gobbi, and G. Mastinu, "Measuring the inertia tensor of vehicles," *Vehicle System Dynamics*, vol. 37, no. sup1, pp. 301–313, 2002.

[44] G. J. Heydinger, D. A. Coovert, R. Lawrence, J. A. Nowjack, N. J. Durisek, and D. A. Guenther, "An overview of a vehicle inertia measurement facility," in *International Symposium on Automotive Technology and Automation (ISATA), 27th, 1994, Aachen, Germany*, 1994.

[45] G. J. Heydinger, N. J. Durisek, D. A. Coovert, D. A. Guenther, and S. J. Novak, "The design of a vehicle inertia measurement facility," SAE Technical Paper, Tech. Rep., 1995.

[46] R. A. Bixel, G. J. Heydinger, N. J. Durisek, D. A. Guenther, and S. J. Novak, "Developments in Vehicle Center of Gravity and Inertial Parameter Estimation and Measurement," SAE Technical Paper, Tech. Rep., 1995.

[47] O. Jonson and E. Endres, "Correlation Work on Shaker Rig Tests and Simulations," Master's thesis, Chalmers University of Technology, Sweden, 2016.

[48] M. Johnston, "Development and evaluation of vehicle suspension tuning metrics," Ph.D. dissertation, University of Windsor, Canada, 2010.

[49] ABDynamics, "Kinematics and Compliance Test Machine," http://www.abd-mf-jp.com/item/spmm/index_e.html, retrieved: 2017.06.06.

[50] V. group, "Endurance testing," http://www.songrock.com.tw, retrieved: 2017.06.06.

[51] H. Wieringa, *Mechanical problems in measuring force and mass*. Springer Science & Business Media, 2012, vol. 3.

[52] M. K. Salaani, "Analytical Tire Forces and Moments with Physical Parameters 2," *Tire science and Technology*, vol. 36, no. 1, pp. 3–42, 2008.

[53] E. M. Kasprzak and D. Gentz, "The formula sae tire test consortium-tire testing and data handling," SAE Technical Paper, Tech. Rep., 2006.

[54] C. Nuthong, "Estimation of Tire-Road Friction Forces using Kalman Filtering for Advanced Vehicle Control," Ph.D. dissertation, München, Germany, 2009.

[55] OnTestAutomation, "Testing in wind tunnel," http://www.ontestautomation.com/why-service-virtualization-is-like-a-wind-tunnel/wind-tunnel-testing/, retrieved: 2017.06.06.

[56] H. Chowdhury, H. Moria, A. Ali, I. Khan, F. Alam, and S. Watkins, "A study on aerodynamic drag of a semi-trailer truck," *Procedia Engineering*, vol. 56, pp. 201–205, 2013.

[57] G. M. Le Good, M. A. Passmore, and A. Cogotti, "A comparison of on-road aerodynamic drag measurements with wind tunnel data from Pininfarina and MIRA," 1998.

[58] J. Qu and G. Huang, "Influence of objective function on parameter identification result," in *Electric Information and Control Engineering (ICEICE), 2011 International Conference on*. IEEE, 2011, pp. 2274–2277.

[59] M. Cavazzuti, "Deterministic optimization," in *Optimization Methods*. Springer, 2013, pp. 77–102.

[60] C. P. Vyasarayani, T. Uchida, A. Carvalho, and J. McPhee, "Parameter identification in dynamic systems using the homotopy optimization approach," in *Identification for Automotive Systems*. Springer, 2012, pp. 129–145.

[61] R. Masoudi, T. Uchida, and J. McPhee, "Parameter estimation of an electrochemistry-based lithium-ion battery model," *Journal of Power Sources*, vol. 291, pp. 215–224, 2015.

[62] R. Masoudi, N. L. Azad, J. McPhee *et al.*, "Parameter Identification of a Quasi-Dimensional Spark-Ignition Engine Combustion Model," SAE Technical Paper, Tech. Rep., 2014.

[63] H. Pacejka, *Tire and vehicle dynamics*. Elsevier, 2005.

[64] dSPACE, "ASM Vehicle Dynamics Brochure," https://www.dspace.com/files/pdf1/ASM-VehicleDynamics_E_ebook.pdf, retrieved: 2017.06.06.

[65] M. A. Emam, "A New Empirical Formula for Calculating Vehicles' Frontal Area," SAE Technical Paper, Tech. Rep., 2011.

[66] Toyota, "2015 Prius product information," https://pressroom.toyota.com/releases/toyota+2015+prius+product+specs.download, retrieved: 2017.06.06.

[67] S. V. D. S. Committee, "Vehicle Dynamics Terminology," *Society of Automotive Engineers*, 2008.

[68] G. Rill, "First order tire dynamics," in *Proceedings of the III European Conference on Computational Mechanics Solids, Structures and Coupled Problems in Engineering, Lisbon, Portugal*, vol. 58, 2006.

[69] J. P. Maurice and H. B. Pacejka, "Relaxation length behaviour of tyres," *Vehicle System Dynamics*, vol. 27, no. S1, pp. 339–342, 1997.

[70] M. S. Corporation, "Adams/car product datasheet," http://media.mscsoftware.com/sites/default/files/ds_adams-car_ltr_w.pdf, retrieved: 2017.06.06.

[71] J. J. McPhee, "On the use of linear graph theory in multibody system dynamics," *Nonlinear Dynamics*, vol. 9, no. 1, pp. 73–90, 1996.

Appendix A

Model parameters and initial conditions

A.1 Tire model parameters

For explanation to x, y and z directions, refer to Fig. 3.1. The values of BCD, C, D, E, S_h, and S_v obtained from the curve fitting (see Section 5.6) with normalized longitudinal force data are represented as $PKx1$, $PCx1$, $PDx1$, $PEx1$, $PHx1$, and $PVx1$ respectively. Similarly, the values of BCD, C, D, E, S_h, and S_v obtained from the curve fitting of normalized lateral force data are represented as $PKy1$, $PCy1$, $PDy1$, $PEy1$, $PHy1$, and $PVy1$ respectively.

Parameter	**Value**	**Description**
Fz0	4700 N	Nominal normal force
R0	0.3175 m	Unloaded radius
V0	15 m/s	Reference velocity
$Lfz0$	1	Scale factor for nominal load
LCx	1	Scale factor for Fx shape factor

$L\mu x$	1	Scale factor for Fx peak friction coefficient
LEx	1	Scale factor for Fx curvature factor
LKx	1	Scale factor for Fx slip stiffness
LHx	1	Scale factor for Fx horizontal shift
LVx	1	Scale factor for Fx vertical shift
$L\gamma x$	1	Scale factor of chamber for Fx
LCy	1	Scale factor for Fy shape factor
$L\mu y$	1	Scale factor for Fy peak friction coefficient
LEy	1	Scale factor for Fy curvature factor
LKy	1	Scale factor for Fy cornering stiffness
LHy	1	Scale factor for Fy horizontal shift
LVy	1	Scale factor for Fy vertical shift
$L\gamma y$	1	Scale factor for camber for Fy
$Ltrail$	1	Scale factor of peak pneumaic trail
$Lres$	1	Scale factor for offset of residual torque
$L\gamma z$	1	Scale factor of camber for Mz
$LX\alpha$	1	Scale factor of slip angle influence on Fx
$LY\kappa$	1	Scale factor of longitudinal slip influence on Fy
$LVy\kappa$	1	Scale factor of longitudinal slip influence on Fy vertical shift
LS	1	Scale factor of moment arm of Fx about vertical axis
LMx	1	Scale factor of overturning couple
$LVMx$	1	Scale factor of Mx vertical shift
LMy	1	Scale factor of rolling resistance torque
PCx1	2.6	Shape factor for longitudinal force
PDx1	0.94	Longitudinal friction, μx, at $Fz0$ and zero inclination
$PDx2$	0	Variation of friction, μx, with load
$PDx3$	0	Variation of friction, μx, with inclination
PEx1	1.1	Longitudinal curvature EFx at $Fz0$
$PEx2$	0	Variation of curvature EFx with load
$PEx3$	0	Variation of curvature EFx with load squared
$PEx4$	0	Brake/drive asymmetry factor for EFz

PKx1	16.65	Longitudinal slip stiffness $\frac{Kfx}{Fz}$ at $Fz0$
$PKx2$	0	Variation of slip stiffness $\frac{Kfx}{Fz}$ with load
$PKx3$	0	Exponent in slip stiffness $\frac{Kfx}{Fz}$ with load
PHx1	0	Horizontal shift of longitudinal slip at $Fz0$
$PHx2$	0	Variation of horizontal shift with load
PVx1	-0.15	Vertical shift at $Fz0$
$PVx2$	0	Variation of vertical shift with load
$RBx1$	10	Slope factor for combined slip Fx reduction
$RBx2$	6	Variation of slope Fx reduction with longitudinal slip
$RCx1$	1.092	Shape factor for combined slip Fx reduction
$REx1$	0	Curvature factor for combined slip Fx reduction
$REx2$	0	Variation of curvature factor with load
$RHx1$	0.007	Shift factor for combined slip Fx reduction
$QSx1$	0	Vertical force induced overturning moment
$QSx2$	0	Camber induced overturning couple
$QSx3$	0	Aligning moment induced overturning couple
PCy1	1.698	Shape factor for pure lateral force
PDy1	-1	Lateral peak fricion, μy
$PDy2$	0	Variation of μy with load
$PDy3$	0	Variation of μy with inclination squared
PEy1	0	Lateral force curvatuire factor at $Fz0$
$PEy2$	0	Variation of curvature with load
$PEy3$	0	Dependency of curvature on the sign of slip angle
$PEy4$	0	Variation of curvature with camber
PKy1	20.03	Maximum value of cornering stiffness $\frac{KMz}{F_{znom}}$
$PKy2$	2.13	Variation of KMz with load
$PKy3$	0	Variation of KMz with camber
PHy1	0	Horizontal shift of lateral force at $Fz0$
$PHy2$	0	Variation of horizontal shift with load
$PHy3$	0	Variation of horizontal shift with camber
PVy1	-0.073	Vertical shift $\frac{Svy}{Fz}$ at $Fz0$

$PVy2$	0	Variation of vertical shift with load
$PVy3$	0	Variation of vertical shift with camber
$PVy4$	0	Variation of vertical shift with camber and load
$RBy1$	6.461	Slope factor for combined slip Fy reduction
$RBy2$	4.196	Variation of slope factor with slip angle
$RBy3$	-0.015	Shift term for alpha in slope factor
$RCy1$	1.081	Shape factor for combined slip Fy reduction
$REy1$	0	Curvature factor for combined slip Fy reduction
$REy2$	0	Variation of curvature factor with load
$RHy1$	0.009	Shift factor for combined slip Fy reduction
$RHy2$	0	Variation of shift factor with load
$RVy1$	0.053	Longitudinal slip induced side forces at $Fz0$
$RVy2$	-0.073	Variation of vertical shift with load
$RVy3$	0.517	Variation of vertical shift with camber
$RVy4$	35.44	Variation of vertical shift with slip angle
$RVy5$	1.9	Variation of vertical shift with longitudinal slip
$RVy6$	-10.71	Variation of vertical shift with arctan(S)
QSy1	0.012	Rolling resistance torque coefficient
$QSy2$	0.00012	Rolling resistance induced by Fx
$QSy3$	0	Rolling resistance induced by V_{Cx}
$QSy4$	0	Rolling resistance induced by V_{Cx}^4
$QBz1$	8.964	Pneumatic trail slope factor, Bt, at $Fz0$
$QBz2$	-1.106	Variation of Bt with load
$QBz3$	-0.842	Variation of Bt with load squared
$QBz4$	-0.227	Variation of Bt with camber
$QBz5$	0	Variation of Bt with absolute camber
$QBz9$	18.47	Slope factor for residual torque Br
$QBz10$	0	Slope factor for residual torque Br
$QCz1$	1.18	Shape factor for pneumatic trail
$QDz1$	0.1	Controls peak pneumatic trail, Dt
$QDz2$	-0.001	Variation of peak Dt with load

$QDz3$	0.007	Variation of peak Dt with camber
$QDz4$	13.05	Variation of peak Dt with camber squared
$QDz6$	-0.008	Controls peak residual torque, Dr
$QDz7$	0	Variation of peak Dr with load
$QDz8$	-0.296	Variation of peak Dr with camber
$QDz9$	-0.009	Variation of peak Dr with camber and load
$QEz1$	-1.608	Pneumatic trail curvature at $Fz0$
$QEz2$	-0.359	Variation of trail curvature with load
$QEz3$	0	Variation of trail curvature with load squared
$QEz4$	0.174	Variation of trail curvature with sign of α
$QEz5$	-0.896	Variation of trail curvature with γ and sign of α
$QHz1$	0.007	Pneumatic trail horizontal shift at $Fz0$
$QHz2$	-0.002	Variation of trail horizontal shift with load
$QHz3$	0.147	Variation of trail horizontal shift with γ
$QHz4$	0.004	Variation of trail horizontal shift with γ and load
$SSz1$	0.043	Nominal value of $\frac{S}{R_0}$: effect of Fx on Mz
$SSz2$	0.001	Variation of S with Mz
$SSz3$	0.731	Variation of S with camber
$SSz4$	-0.238	Variation of S with camber and load

Table A.1: PAC 2002 tire model parameters of the Prius

The values of parameters indicated in bold in A.1 are estimated from the experimental data of the Prius.

A.2 Vehicle model parameters

Complete list of parameters that are used for the full vehicle simulation are shown in the Table below.

Parameter	**Value**	**Unit**	**Description**
M	1631	kg	Mass of the vehicle
L	2.7	m	Wheel base
W	1.72	m	Track width
r	3.267	-	Final drive ratio
A_f	2.19	m^2	Frontal area
C_d	0.25	-	Coefficient of drag
f_{rr}	0.012	-	Rolling resistance coefficient
h	0.60	m	CG height
L_r	1.46	m	Longitudinal location of CG from rear wheels
I_x^*	1000	kgm^2	Roll inertia of the vehicle w.r.t CG
I_y	2888	kgm^2	Pitch inertia of the vehicle w.r.t CG
I_z^*	3000	kgm^2	Yaw inertia of the vehicle w.r.t CG
m_w	18	kg	Mass of each wheel
J_w	1.67	kgm^2	Wheel inertia
d_x^*	500	$\frac{Ns}{m}$	Longitudinal tire damping coefficient
d_y^*	400	$\frac{Ns}{m}$	Lateral tire damping coefficient
d_z^*	500	$\frac{Ns}{m}$	Vertical tire damping coefficient
C_x	169700	N	Longitudinal tire stiffness
C_y	120000	N	Lateral tire stiffness
K_t	281235	$\frac{N}{m}$	Vertical tire stiffness
K_f	31052	$\frac{N}{m}$	Front suspension stiffness
K_r	24321	$\frac{N}{m}$	Rear suspension stiffness
C_f	2019	$\frac{Ns}{m}$	Front suspension damping
C_r	2088	$\frac{Ns}{m}$	Rear suspension damping
SR	20	-	Steering ratio
J_d	0.07	kgm^2	Driveline inertia

K_{hs}	29292 and 16576	$\frac{Nm}{rad}$	Torsional stiffness of left and right half shaft
d^*_{hs}	100 and 100	$\frac{Nms}{rad}$	Torsional damping of left and right half shafts
SF_f	6.1	-	Scale factor for front brakes
SF_r	2.4	-	Scale factor for rear brakes
S_{max}	0.15	-	Maximum slip for ABS
S_{min}	0.06	-	Minimum slip for ABS

Table A.2: Vehicle dynamics model parameters of the Prius

$*$ indicates the values that are not estimated in Chapter 5.